Title
Gut bacterial nutrient preferences quantified in vivo

Journal
Cell, 185(18)

ISSN
0092-8674

Authors
Zeng, Xianfeng
Xing, Xi
Gupta, Meera
et al.

Publication Date
2022-09-01

DOI
10.1016/j.cell.2022.07.020

Peer reviewed

HHS Public Access

Author manuscript

Cell. Author manuscript; available in PMC 2023 September 01.

Published in final edited form as:

Cell. 2022 September 01; 185(18): 3441–3456.e19. doi:10.1016/j.cell.2022.07.020.

Gut bacterial nutrient preferences quantified in vivo

Xianfeng Zeng[1,4], **Xi Xing**[1,4], **Meera Gupta**[2,3,4], **Felix C. Keber**[2,4], **Jaime G. Lopez**[4], **Ying-Chiang J. Lee**[2], **Asael Roichman**[1,4], **Lin Wang**[1,4,6], **Michael D. Neinast**[1,4], **Mohamed S. Donia**[2], **Martin Wühr**[2,4,†], **Cholsoon Jang**[5,†], **Joshua D. Rabinowitz**[1,4,7,8,†]

[1]Department of Chemistry, Princeton University, Princeton, New Jersey 08544, USA

[2]Department of Molecular Biology, Princeton University, Princeton, New Jersey 08544, USA

[3]Department of Chemical and Biological Engineering, Princeton University, Princeton, NJ 08544, USA

[4]Lewis-Sigler Institute for Integrative Genomics, Princeton University, Princeton, New Jersey 08544, USA

[5]Department of Biological Chemistry, University of California Irvine, Irvine, California 92697, USA

[6]Institute of Basic Medical Sciences, Chinese Academy of Medical Sciences & Peking Union Medical College, No. 5 Dong Dan San Tiao, Dongcheng District, Beijing 100005, China

[7]Ludwig Institute for Cancer Research, Princeton Branch, Princeton University, Princeton, NJ 08544, USA

[8]Lead contact

SUMMARY

Great progress has been made in understanding gut microbiome's products and their effects on health and disease. Less attention, however, has been given to the inputs that gut bacteria consume. Here we quantitatively examine inputs and outputs of the mouse gut microbiome, using isotope tracing. The main input to microbial carbohydrate fermentation is dietary fiber, and to branched-chain fatty acids and aromatic metabolites is dietary protein. In addition, circulating host lactate, 3-hydroxybutyrate and urea (but not glucose or amino acids) feed the gut microbiome. To determine nutrient preferences across bacteria, we traced into genus-specific bacterial protein

†Correspondence: joshr@princeton.edu, choljang@uci.edu, wuhr@princeton.edu.

AUTHOR CONTRIBUTIONS. X.Z., and J.D.R came up with general approach. X.Z. performed most of the experiment and data analysis. C.J. worked intensively with X.Z. to develop the experimental strategy. M.W. designed and enabled the proteomic measurements. X.X. wrote the MATLAB code. M.G., F.C.K., and M.D.N. contributed to proteomics method development. J.G.L. and M.S.D. provided microbiome expertise and performed 16S rRNA gene amplicon sequencing. Y.-C.J.L. performed *in vitro* bacterial culture studies. A.R. assisted with isotope tracing. L.W. performed ammonia measurement. X.Z., C.J., and J.D.R. wrote the paper. All the authors discussed the results and commented on the paper.

DECLARIATION OF INTERESTS. J.D.R. is a member of the Rutgers Cancer Institute of New Jersey and the University of Pennsylvania Diabetes Research Center; a co-founder and stockholder in Empress Therapeutics and Serien Therapeutics; and advisor and stockholder in Agios Pharmaceuticals, Bantam Pharmaceuticals, Colorado Research Partners, Rafael Pharmaceuticals, Barer Institute and L.E.A.F. Pharmaceuticals. M.S.D. is a member of the scientific advisory board of DeepBiome Therapeutics and VastBiome.

sequences. We find systematic differences in nutrient use: Most genera in the phylum Firmicutes prefer dietary protein, *Bacteroides* dietary fiber, and *Akkermansia* circulating host lactate. Such preferences correlate with microbiome composition changes in response to dietary modifications. Thus, diet shapes the microbiome by promoting the growth of bacteria that preferentially use the ingested nutrients.

Graphical Absctract

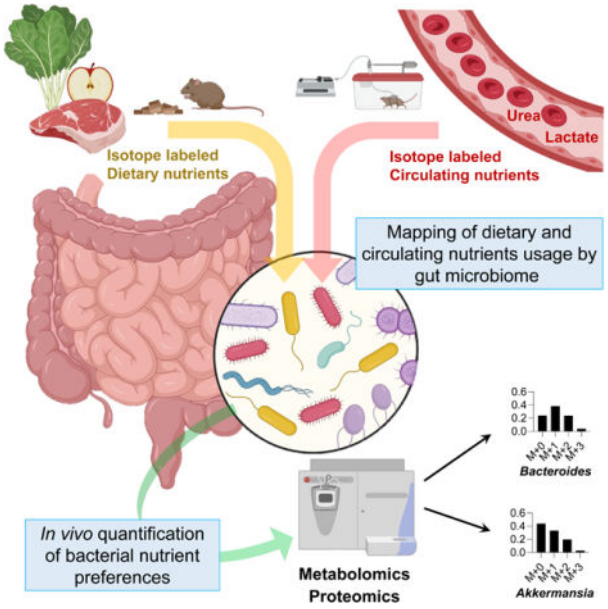

In Brief:

Isotope tracing into bacterial-specific protein sequences allows for a determination of nutrient preferences across gut microbes *in vivo*, and reveals how diet alters microbiome composition.

INTRODUCTION

The gut microbiome possesses an enormous diversity of enzymes, exceeding the number in mammals' genomes by more than 100-fold (Qin et al., 2010). This enzymatic capacity enables the processing of incoming dietary nutrients into a broad spectrum of microbial metabolites. Some of these reach the host circulation at substantial concentrations (Lai et al., 2021; Quinn et al., 2020). Microbial metabolites can play important roles in host pathophysiology. For example, short-chain fatty acids (SCFAs; acetate, propionate, butyrate) (Dalile et al., 2019; Koh et al., 2016), trimethylamine N-oxide (Tang et al., 2013), secondary bile acids (Arab et al., 2017; Funabashi et al., 2020), indole-3-propionate (Wikoff et al., 2009), and imidazole propionate (Koh et al., 2018) affect immune maturation (Campbell et al., 2020; Hang et al., 2019), insulin sensitivity (Koh et al., 2018), cancer growth (Garrett, 2015; Yoshimoto et al., 2013), and cardiovascular disease (Nemet et al., 2020; Wang et al., 2011).

Both to replicate themselves and to release metabolic products, gut bacteria require nutrient inputs. These come in forms including ingested food, host-synthesized gut mucus (Desai et al., 2016; Sicard et al., 2017), and host circulating metabolites (Scheiman et al., 2019). The availability of dietary nutrients to gut microbiota depends on the extent of host absorption: nutrients that are absorbed in the small intestine, like starch, are not available to the colonic microbiome. In contrast, nutrients that are poorly digested in the upper gastrointestinal tract, like fiber, can be key microbiome feedstocks (Lund et al., 2021; Wong and Jenkins, 2007).

Isotope tracing enables quantitative measurement of the inputs to metabolites and biomass. Studies employing radioactive tracers defined the basics of mammalian metabolism (Wolfe, 1984). Recent work has increasingly relied on stable isotope tracers coupled to mass spectrometry detection, which enables the measurement of labeling in specific downstream products (Fernández-García et al., 2020; McCabe and Previs, 2004). This approach has revealed fundamental features of host metabolism, such as circulating lactate being a major TCA fuel (Faubert et al., 2017; Hui et al., 2017). In addition, it has provided important insights into host-microbiome metabolic interplay. For example, it revealed that dietary fructose is processed by the microbiome into acetate, which fuels hepatic lipogenesis (Jang et al., 2018; Zhao et al., 2020).

In principle, stable isotope tracing coupled to mass spectrometry can also be applied to determine the metabolic inputs to specific microbes, based on measuring labeling in bacteria-specific peptide sequences (Berry et al., 2015; Holmes et al., 2017; Oberbach et al., 2017; Reese et al., 2018; Zhang et al., 2016a, 2016b). By infusing nitrogen-labeled threonine to label host mucus, investigators were able to compare the contribution of dietary versus mucus protein to the gut microbiome and observed a shift towards more mucus contribution in mice fed a low-protein diet (Holmes et al., 2017).

Here, we perform large-scale, quantitative assessment of the metabolic inputs to the gut microbiome and its products. We examine the contributions from dietary starch, fiber, and protein, and from host mucus. We also examine most major circulating host nutrients, finding that lactate, 3-hydroxybutyrate, and urea stand out for passing from the host to the gut microbiome. Based on the measurement of bacteria-specific peptide sequences, we assess the nutrient preferences of different bacterial genera and show that these preferences align with microbiome composition changes in response to altered diet.

RESULTS

Microbiome consumes less digestible dietary components

A major mechanism by which the microbiome may impact host physiology is via secreted metabolic products. We measured, in the portal, systemic circulation and the cecal contents, the absolute concentrations of more than 50 metabolites characterized in the literature as microbiome-derived (Campbell et al., 2020; De Vadder et al., 2014; Han et al., 2021; Hang et al., 2019; Koh et al., 2018; Mager et al., 2020; Ridlon et al., 2014; Wikoff et al., 2009) (Figure S1A-B, Table 1, S1). Most were elevated in the portal circulation relative to systemic blood, and all but two (inosine and N-acetyl-tryptophan, which are apparently mainly host derived) were depleted by antibiotics treatment.

The dominant excreted products on a molar basis (0.4 – 2 mM in the portal blood) are SCFAs. Other relatively abundant microbiome products (10 – 30 uM) are aromatic amino acid fermentation products (phenol, indoxyl sulfate, and 3-phenylpropionate) and branched-chain fatty acids (valerate, isovalerate, 4-methylvalerate, isobutyrate, 2-methylbutyrate). Primary bile acids, while present in the portal circulation at up to ~ 10 uM concentration, are produced by the host and accordingly were not included in Table 1. Secondary bile acids, which are produced from primary bile acids by the microbiome, were lower in absolute concentration, the most abundant being tauroursodeoxycholic acid (3 uM in portal vein).

To probe the dietary inputs to gut microbial products, we began by feeding mice via oral gavage, starch (readily digestible glucose polymer) and inulin (slowly digestible fructose polymer, i.e., soluble fiber) (Figure S1C). Following ^{13}C-starch gavage, labeled glucose, lactate, and alanine quickly appeared in the portal circulation and accounted for most starch carbons (~75%) (Figure S1D–F, S1G) (Jang et al., 2018). In contrast, after ^{13}C-inulin gavage, substantial labeled fructose, glucose, lactate, and alanine were not observed, and instead labeled portal metabolites slowly appeared in the form of SCFAs, with ~ 40% of inulin carbons becoming SCFAs and the remainder being undigested and excreted in the feces (Figure S1E–F, S1H–I). Moreover, dietary inulin, but not starch, extensively labeled glycolytic and TCA intermediates and amino acids in the cecal content (Figure S1G).

We next carried out similar experiments, comparing the gavage of a free amino acid mixture to algal protein, both uniformly ^{13}C-labeled (Figure S1C). The free amino acids resulted in the rapid appearance of labeled amino acids in portal circulation (Figure S1J–L), while the algal protein substantially labeled amino acids within the cecal contents (Figure S1M). Moreover, the algal protein copiously labeled microbiome-derived portal vein metabolites: SCFAs, branched-chain fatty acids, and aromatics (indole, indole-3-propionate, 3-phenylpropionate) (Figure S1K–L). Thus, poorly digestible carbohydrates and protein feed the microbiome directly, and the host indirectly via microbiome-derived products.

Few circulating metabolites reach the microbiome

Next, we examined the possibility that nutrients in host circulation feed the gut microbiota. We infused deuterated water and eighteen major circulating nutrients (^{13}C-labeled) into the systemic circulation of pre-catheterized mice (Figure 1A). The infusion rates were selected to achieve modest but readily measurable labeling without substantially perturbing circulating concentrations. Circulating labeling reached a steady state by 2.5 h, at which time we collected serum and feces to quantitate the carbon contributions of each circulating nutrient to the corresponding fecal metabolites. Upon intravenous infusion of ^{13}C-lactate, fecal lactate labeled rapidly (Figure 1B). Most infused circulating nutrients, however, did not penetrate the feces (Figure 1C–D). Indeed, while water fully exchanged with the feces, among abundant circulating carbon carriers, only lactate and 3-hydroxybutyrate penetrated. Glucose, amino acids, TCA intermediates and fatty acids did not. Both lactate and 3-hydroxybutyrate are substrates of monocarboxylate transporters (MCTs), which are highly expressed in the colonic epithelium (Halestrap and Price, 1999, p. 1). Pharmacological MCT inhibition prevented lactate from penetrating the feces (Figure 1E). Thus, in contrast to most

host circulating metabolites, which do not reach the colonic microbiome, monocarboxylic transporters render circulating lactate and 3-hydroxybutyrate accessible to gut microbes.

Circulating urea is a microbiome nitrogen source

In addition to carbon, nitrogen is a fundamental constituent of all living cells. To assess nitrogen sources of the gut microbiome, we infused twelve abundant circulating nutrients in ^{15}N-labeled form. Nitrogen from circulating urea and ammonia, but not amino acids, penetrates the feces and contributes to microbiome amino acids and ammonia (Figure 1F, S2A–B). Urea usage by the microbiome involves its re-conversion to ammonia via the enzyme urease, which is expressed by a subset of gut microbes (Mora and Arioli, 2014; Ni et al., 2017), and gnotobiotic mice colonized intentionally with only urease-negative bacteria showed no labeling from urea (Figure S2C-D).

Urea, which is made from ammonia in the liver, was a quantitatively greater source of microbiome nitrogen than ammonia. Moreover, urea but not ammonia was more abundant in the host circulation than cecal lumen, consistent with only urea being able to passively flow into the gut lumen (Figure S2E–F). We hypothesized that circulating host ammonia might be feeding the microbiome mainly indirectly, after being converted by the host liver into circulating urea (Figure S2G) (Bartman et al., 2021). This indirect contribution was calculated by multiplying circulating urea's contribution to fecal amino acids ($L_{AAs \leftarrow urea}$) by the circulating urea fraction that comes from circulating ammonia ($L_{urea \leftarrow NH_3} = 33\%$).

It fully explained the observed microbiome labeling from circulating ammonia (Figure S2H). Further supporting the indirect pathway, antibiotics treatment blocked both circulating urea and ammonia from becoming cecal ammonia (Figure S2I–J), which makes sense if flux of ammonia into the cecal contents goes through host urea and microbial urease (Figure S2K).

Microbiota synthesize amino acids from fiber and urea

To determine quantitatively the sources of microbiome metabolites, we measured their labeling after *ad libitum* feeding of isotopically enriched food. To this end, we fed mice standard chow with a portion of the fiber, fat, or protein ^{13}C-labeled, with cecal labeling reaching steady-state within 12 h (Figure S3A). To account for circulating nutrient inputs, we also infused ^{13}C-lactate or 3-hydroxybutyrate (Figure 2A). These studies identified a majority of the carbon feeding into most microbiome central metabolites, with glycolytic and pentose phosphate metabolites labeling almost exclusively coming from dietary fiber (inulin), while pyruvate and TCA metabolites are also labeled from dietary protein and circulating lactate (Figure 2B and S4A).

We next examined inputs to microbiome free amino acids, tracing also with ^{15}N-labeled dietary protein and infused urea. Unlike mammals, most gut bacteria have the biosynthetic capacity to make all 20 proteogenic amino acids. Nevertheless, we observed that "essential amino acids," which cannot be made by mammals and require the expression of extensive biosynthetic pathways in bacteria, are derived mainly from dietary proteins (Figure 2C). In contrast, "non-essential amino acids" are primarily synthesized within the gut microbiome, using dietary inulin and circulating lactate as carbon sources. Microbiota depletion with

antibiotics or in germ-free mice favored cecal accumulation of those amino acids coming (based on our isotope tracing studies) largely from dietary protein, and depletion of those being synthesized by the microbes (Figure S3B–G).

Dietary protein was the main nitrogen source for both essential and non-essential amino acids, with host urea also contributing substantially to the non-essential amino acids (Figure 2D). Dietary protein provides nitrogen to cecal amino acids mainly directly, not through circulating urea (Figure S3H–I). Consistent with the gut microbiome synthesizing amino acids from fiber carbon and urea nitrogen, across amino acids, urea's nitrogen contribution correlated with inulin's carbon contribution (Figure 2E).

Amino acid labeling from inulin was typically partial (i.e., one or a few of the amino acid's carbons atoms were labeled), reflecting inulin's carbons being scrambled with other inputs into central metabolism (Figure S3J). In contrast, labeling from ^{13}C, ^{15}N-proteins were typically complete (or complete except for the nitrogen label, Figure S3K), indicating direct usage of intact amino acids after proteolysis (sometimes after a cycle of deamination and re-amination). Consistent with such re-amination, the combination of ^{15}N-urea infusion and ^{13}C-protein feeding produced some double-labeled (^{13}C,^{15}N-labeled) amino acids (Figure S3L).

Lastly, the amino acids synthesized by the microbiome, stay in the microbiome: We do not observe discernible labeling of these amino acids in the host (Figure S3M). Taken together, we found that: (i) essential amino acids, although capable of being synthesized by the microbiome, come mainly from the diet and do not go through any carbon rearrangements, (ii) the most closely TCA-linked non-essential amino acids are substantially synthesized by the microbiome using carbon from fiber scrambled with other carbon via central metabolic reactions, and (iii) transamination reactions partially mix nitrogen from diet-derived amino acids with nitrogen from host urea.

Diverse microbiome products come from dietary protein

We next examined the carbon inputs to the other major microbiome products, especially the ones excreted into the portal circulation (Table 1). As expected, SCFAs, the most abundant microbial metabolites, come mainly from dietary fiber. Many less abundant ones, however, are mainly derived from dietary protein (Table 1).

In addition to classical microbiome products, we also observed metabolites that are made in a collaborative manner, with the host carrying out the final synthesis using microbiome-derived inputs. For example, a wide range of microbiome-derived carboxylic acids are conjugated to glycine in the liver and the kidneys to make different acyl-glycines (Figure S4B–E) (Wikoff et al., 2009).

We also examined the host clearance mechanisms of microbiome metabolites, based on arterial-venous gradients across the liver and kidney and levels in the urine. SCFAs and branched-chain fatty acids were avidly consumed by the liver. Most microbiome-derived metabolites were excreted by the kidney into the urine, with the notable exception of SCFAs, which are actively reabsorbed (Table S1A) (Jang et al., 2019; Ullrich et al., 1982). Thus, we

establish dietary protein as a major precursor to many microbiome metabolites and identify host-microbiome interplay in the metabolism of SCFAs, including their renal reabsorption and use by liver and kidney for the synthesis of acyl-glycines.

Circulating levels of microbiota metabolites are controlled by protein digestibility

We found that many microbiome-derived metabolites are derived from unabsorbed dietary protein that reaches the colon. We hypothesized that the circulating levels of such metabolites would depend on the extent of dietary protein reaching the colon microbiome. To manipulate this, we fed mice diets in which a portion of the protein (casein, which in part reaches the colonic microbiome) was replaced with free amino acids (which are essentially fully absorbed in the small intestine) (Figure 3A). After 2 weeks, we performed metabolomics on the systemic blood. As expected, diets with less intact protein and more free amino acids tended to increase circulating amino acid levels (Figure 3B). Importantly, protein-derived circulating microbial metabolites (phenols, indoles, and acyl-glycines) fell in tandem (Figure 3C–I). Thus, knowledge of the nutrient sources of microbiome metabolites can be applied to manipulate their systemic levels.

Gut bacterial growth is synchronized with host feeding

Thus far, we have reported inputs and outputs of the gut microbiome as a whole. We now shift to examining the growth and metabolism of specific bacterial genera. To this end, we deployed proteomics to measure gut microbial peptides and their labeling, focusing on peptide sequences specific to a single bacterial genus (Figure 4A).

To quantify protein synthesis in different gut microbial genera, we used deuterated water (D_2O) tracing (Holmes et al., 2015; O'Brien et al., 2020). To achieve steady-state labeling of body water, we gave mice D_2O by bolus injection followed by mixing it into drinking water. Peptide labeling in the cecal contents was then measured by proteomics (Figure 4B).

A key technical challenge in using proteomics to read out metabolic activity is the complexity, arising from natural isotope abundances, of peptide mass spectra. We used liquid chromatography-high resolution mass spectrometry to obtain the full scan (MS1) mass isotope distribution for each peptide of interest, with MS/MS analysis of the unlabeled form used to determine the peptide's identity. We then calculated, based on the mass isotope distribution, the fraction of peptide that was newly synthesized (θ). To this end, first, we calculated the mass isotope distribution of unlabeled peptides based on natural isotope abundances ("old"). Second, we calculated the expected mass isotope distribution of a newly-synthesized peptide generated from cecal free amino acids, whose labeling we experimentally measured by metabolomics. Then, we determined the fraction of newly synthesized (θ) by linear interpolation between the "old" and "newly synthesized" spectra (Figure 4C). To verify this approach *in vitro*, we cultured *Clostridium sporogenes* and *Bacteroides dorei* in media enriched with D_2O and measured growth rate as is typically done (based on OD_{600}) and as above (using media in place of cecal amino acid labeling), finding good agreement (Figure S5A–C).

We then measured the newly synthesized fraction (θ) for a minimum of 5 peptides for each bacterial genus *in vivo*, with abundant gut bacteria yielding θ for over 100 characteristic

peptides. Irrespective of their intracellular location, different peptides from the same bacterial genus tended to label at a similar rate (Figure 4D, S5D–E). Labeling rate varied across bacterial genera, with a half doubling time ranging from 2.5 h for *Akkermansia* to 8 h for *Lactobacillus*, which still markedly exceeded the labeling rate of host intestinal proteins (> 24 h half doubling time) (Figure 4E–F, Figure S5F).

Our prior analyses revealed that the microbiome is fed substantially by dietary components. Accordingly, we hypothesized that microbial growth synchronizes with physiological feeding, which in mice occurs mainly during the nighttime. To assess the diurnal rhythm of gut bacterial protein synthesis, mice were given D_2O for 6 h intervals throughout the diurnal cycle, followed by proteomic analysis of their cecal contents. Every measured bacterial genus showed greater protein synthesis during nighttime than daytime (Figure 4G). Thus, gut bacteria grow in sync with the physiological feeding patterns of the host.

Preferred carbon sources differ across gut bacteria

Next, we quantitated the carbon feedstocks of different microbes, by combining ^{13}C-nutrient labeling and proteomics. Each ^{13}C-labeled nutrient (dietary inulin, dietary algal protein, or circulating lactate) was provided for 24 hours, which is sufficient to achieve steady-state labeling in the gut bacteria. Our analysis strategy involved two steps: first, we calculated, based on each genus-specific peptide's observed mass isotope distribution, its relative ^{13}C-enrichment (γ) compared to that of cecal free amino acids (Figure 5A). Mathematically, this calculation is identical to the calculation of θ in the D_2O case, except here, the tracer is a particular ^{13}C-labeled nutrient, which unlike D_2O is used preferentially by certain bacterial genera. The observed peptide's relative ^{13}C-enrichment multiplied by the average contribution of that ^{13}C-tracer to the gut microbial amino acids pool ($L_{AA\_avg \leftarrow nutrient}$) gives a quantitative measure of the tracer's contribution to the observed genus-specific peptide. Averaging across such peptides gives a fractional contribution of the ^{13}C-labeled nutrient to protein synthesis in a bacterial genus.

Using this method, we measured feedstocks of the bacterial genera that were detected in every proteomics experiment. We were also able to make species-specific measurements in some cases (Figure S6A–F). We observed marked differences in nutrient preferences across microbiota. For example, *Bacteroides* and *Clostridium* use over four-fold more inulin than *Akkermansia*, *Muribaculum,* or *Alistipes* (Figure 5B, S6A). Overall, bacteria from the phylum Firmicutes, used more dietary protein than did Bacteroidetes (Firmicutes 0.237 ± 0.052; Bacteroidetes 0.175 ± 0.031, p = 0.02). *Akkermansia,* which is generally considered a health-promoting gut microbe, used among the least dietary inulin and protein (Figure 5B–C, S6A–B). In contrast, it used by far the most circulating lactate from the host (Figure 5D, S6C).

We were curious whether these bacterial nutrient preferences predict microbiome composition changes upon dietary changes. To explore this possibility, we fed mice an inulin-enriched or algal protein-enriched diet for two days and measured microbiome composition by 16S rRNA gene amplicon sequencing. *Bacteroides,* the top consumer of ^{13}C-inulin, increased by 4-fold after high inulin diet (Figure 5E–G). *Clostridium*, another high inulin consumer, also increased by 2-fold. Other genera that use less inulin carbon

were either unchanged or slightly decreased. Similar consistency between microbes' nutrient preference and abundance changes was observed in mice fed the algal protein-enriched diet (Figure 5H–J). Carbon-source preference measured by proteomics ($f_{genus \leftarrow nutrient}$) correlates with abundance change following a diet shift measured by 16S rRNA gene amplicon sequencing, for both the inulin and algal protein conditions (Figure 5G, J). Thus, the nutrient preferences of different gut bacteria help explain microbiome compositional changes following dietary manipulations (David et al., 2014).

Firmicutes consume dietary protein while Bacteroidetes consume secreted host protein

Lastly, we turned to the nitrogen source preferences of different gut bacteria, comparing ^{15}N-labeled dietary protein feeding to ^{15}N-urea infusion. The analytical approach was identical to that employed above for carbon source preferences. Bacterial genera that highly use carbon from dietary protein also highly use nitrogen from dietary protein, consistent with amino acids from dietary protein being assimilated intact in bacterial proteomes (Figure 6A, S6D, S6G).

Conversely, among members of the phylum Firmicutes, genera preferring urea nitrogen tended to be avid inulin users, i.e., to synthesize their own amino acids using inulin and urea (Figure 6B, S6E, S6H). This includes some urease-negative genera, which presumably acquire urea nitrogen via cross-feeding. Moreover, again among Firmicutes, we also saw the expected trade-off where some genera prefer nitrogen from dietary protein, and others from circulating urea (Figure S6I). Following intravenous urea infusions to raise circulating urea concentrations, abundance of those Firmicutes preferring urea, along with *Akkermansia*, increased substantially (Figure 6C–F).

Compared to Firmicutes, the lower use of both dietary protein and circulating urea nitrogen by Bacteroidetes raised a key question: How do Bacteroidetes get nitrogen? Some members of gut microbiome (e.g. *Bacteroides* and *Akkermansia*) are capable of digesting host secreted proteins such as mucins (Berry et al., 2013; Reese et al., 2018). We hypothesized that host secreted proteins are a key source of Bacteroidetes nitrogen. To probe this possibility, we performed long-term ^{15}N-labeled lysine and arginine infusions (12, 18, 36 h) to label host proteins in the colon (Figure 6G and Figure S7A–E). Despite not directly feeding the microbiome (Figure 1F, S7E), lysine and arginine did contribute after 36-h infusion, consistent with the labeling occurring via host proteins. Such labeling occurred preferentially in Bacteroidetes and *Akkermansia* (Figure 6H, S6F). The nitrogen contributions from dietary and secreted host proteins were anti-correlated, consistent with some gut bacteria preferentially consuming dietary protein, and others host protein (Figure 6I). Bacterial genera with a greater preference for dietary protein, whose availability depends on host feeding, grow more differently between daytime and nighttime (Figure S6J–K). Thus, dietary proteins and circulating urea are the major nitrogen feedstock of Firmicutes, while secreted host proteins provide nitrogen to Bacteroidetes.

DISCUSSION

As for most microbial communities, the composition of the gut microbiome is shaped by nutrient availability. Here we developed quantitative isotope tracing approaches to

measure the nutrient preferences of gut bacteria. In addition to dietary fiber and secreted host proteins, we establish dietary protein and circulating host lactate, 3-hydroxybutyrate, and urea as important nutrients feeding gut bacteria. Importantly, we rule out direct contributions from other circulating host nutrients, like glucose and amino acids, to the colonic microbiome.

A key technical achievement is enabling tracing from different carbon and nitrogen sources into bacteria-specific peptides, thereby revealing the nutrient preferences of different bacteria within the complex and competitive gut lumen environment. We find that Firmicutes and Bacteroidetes differ systematically in their utilization of host secreted protein versus dietary protein: Firmicutes tend to acquire amino acids from dietary protein, while Bacteroidetes rely more on secreted host protein (Figure 6J). This may relate to different localization of bacteria within the colon, either in terms of central versus peripheral (closer to host mucus) or distal versus proximal (closer to incoming food remnants) (Albenberg et al., 2014; Li et al., 2015; Yasuda et al., 2015).

Within these two major families of gut bacteria, we found marked disparities in the use of dietary fiber as a carbon source. The most abundant Bacteroidetes' genus is *Bacteroides,* and it was the most avid assimilator of fiber (inulin). In contrast, other types of bacteria in the same phylum hardly consumed inulin. Likewise, some Firmicutes like *Clostridium* avidly used fiber, while others did not. Strikingly, feeding a fiber-enriched diet led to an increased abundance of *Bacteroides* and *Clostridium,* the precise genera that most actively assimilate fiber based on isotope tracing.

A similar trend was observed in the case of dietary supplementation with algal protein: Firmicutes, which actively use such protein, tended to increase in abundance. Algal protein (the only type commercially available in bulk in ^{13}C-labeled form) may be particularly hard for mammals to digest. This is reflected in the limited appearance of ^{13}C-labeled amino acids from algal protein in the portal circulation, and instead extensive passage from the intestine into the colon. This influx of dietary protein to the microbiome was a major contributor to secreted microbiome metabolites: As shown by replacing intact dietary protein with more absorbable (and thus less microbiome-accessible) free amino acids, the production and hence systemic concentration of these products depends on dietary protein reaching the colonic microbiome. An important future question is whether the nature of dietary protein (e.g. plant or animal-based) impacts passage through the small intestine to the colonic microbiome and thereby shapes microbiome composition or metabolite secretion (Madsen et al., 2017; Wali et al., 2021).

Host circulating metabolite levels may also impact microbiome nutrient access and ultimately composition. Here we show such effects are likely limited to the few host metabolites that meaningfully penetrate the microbiome: urea, 3-hydroxybutyrate, and lactate. Among them, lactate was recently shown to feed the gut microbiome in human marathon runners (Scheiman et al., 2019). Among gut bacteria, *Akkermansia* most avidly use circulating lactate. *Akkermansia* are mucin degraders, and their proximity to the gut epithelial wall may augment their access to lactate from the host circulation. *Akkermansia* are more abundant in athletes, and exercise increases their levels in mice and human (Liu

et al., 2017; Munukka et al., 2018). A possible mechanism involves increased circulating lactate levels following exercise directly feeding *Akkermansia*. Whether lactate induced *Akkermansia* growth in part mediates beneficial effects of exercise is an important open question. Consistent with their urea preferences measured by isotope tracing, *Akkermansia* and certain genera within Firmicutes (e.g., *Roseburia*, *Butyricoccus*, *Ruminococcus*) also increase in abundance upon experimental elevation of circulating host urea.

Ultimately, manipulating the microbiome requires understanding which nutrients different bacteria consume, and how such consumption impacts microbiome composition and product secretion. Through isotope tracing, including proteomic measurements that offer bacterial genus specificity, we provide foundational knowledge about which nutrients feed the gut microbiome, and which bacteria prefer which nutrients. The methodologies developed here are poised for broader application, to eventually contribute to the holistic and quantitative understanding of the diet-microbiome-health connection.

LIMITATIONS OF THE STUDY

Our investigation focuses solely on healthy mice fed standard chow (in some cases with specific fiber or protein supplements). Measurements of microbiome feedstocks are limited to isotope tracing and mass spectrometry. Feedstocks of different bacteria are determined based on the isotopic signatures of bacteria-specific peptides. Peptide identification involves a 2% false discovery rate. Taxonomic assignment is based on bacterial proteome sequences available on Uniprot (Gurdeep Singh et al., 2019). Orthogonal approaches, which could provide measurement validation or complementary information, such as fluorescent-activated cell sorting of bacteria, were not explored (Batani et al., 2019). In most cases, taxonomic assignment was limited to the genus level, due to lack of sufficient specificity of the detected peptide sequences. In the future, improved sensitivity may enable species- or strain-specific peptide sequence measurements.

STAR*METHODS

RESOURCE AVAILABILITY

Lead Contact—Further information and requests for resources and reagents should be directed to and will be fulfilled by the lead contact, Professor Joshua D. Rabinowitz (joshr@princeton.edu).

Materials Availability—This study did not generate new unique regents or new mouse lines.

Data and Code Availability—The proteomics datasets generated during this study are deposited in PRIDE: PXD031015. The isotope tracing data are included in Table S2. The taxonomic assignment of the detected tryptic peptides in the study are included in Table S3. Composition of the diet used in the study are included in Table S4. The 16S rRNA gene amplicon sequencing datasets generated during this study are available in Table S5. The code for peptide enrichment calculations generated during this study is available at GitHub:

(https://github.com/xxing9703/pepMID_simul). Any additional information required to re-analyze the data reported in this work is available from the lead contact upon request.

EXPERIMENTAL MODEL AND SUBJECT DETAILS

Mouse studies.—Mouse studies followed protocols approved by the Princeton University Animal Care and Use Committee. Unless otherwise indicated, 7–9-week-old male C57BL/6NCrl mice (strain 027; Charles River Laboratories) were group-housed on a normal light-dark cycle (8:00–20:00) with free access to water and chow.

Bacterial culture studies.—*B. dorei*, *C. sporogenes, E. coli, S. aureus* and *L. reuteri* glycerol stocks were brought into an anerobic chamber (70% N_2, 25% CO_2, 5% H_2) and grown in liquid media: *L. reuteri* was grown on MRS (MRS Broth, Sigma); *E. coli* was grown on LB (Luria Broth, Sigma); *S.aureus* was grown in TSB (Tryptic Soy Broth, Bacto) and *C. sporogenes* and *B. dorei* were grown in GAM (GAM Broth Modified, HyServe).

METHOD DETAILS

Mouse gavage and nutrient feeding.—For the ^{13}C-nutrient gavage experiments, mice were fasted at 9 am and received a 1:2:4 mixture of inulin, protein/amino acids, and starch (0.5 g kg^{-1} inulin, 1 g kg^{-1} protein/amino acids 2g kg^{-1} starch dissolved in water) at 3 pm via oral gavage with a plastic feeding tube (Instech Laboratories). Food was given back at 8 pm.

For the mouse experiments involving labeled nutrient feeding, the labeled diet was prepared by adding $^{13}C/^{15}N$-nutrients to a diet mixture premix (modified from normal diet with reduced protein, inulin, and starch content, Research diets Inc, D20030303). The final enrichment for each labeled dietary nutrient was 10% - 25% (with observed labeling corrected by dividing by the fraction dietary nutrient labeled). The contribution of each dietary nutrient to metabolites is calculated by the metabolite labeling enrichment normalized to the final enrichment of each labeled dietary nutrient. All diets shared the same final macronutrient composition (40% starch, 20% protein or amino acids, 7.5% inulin and 2.5% cellulose). Mice were first adapted to a non-labeled diet (of identical composition to the subsequent labeled diet) for 10 days, and then fed labeled diet for 24 h prior to sacrifice.

For the deuterium water drinking experiment, mice were administered a bolus intraperitoneal injected of D_2O (1.26 % w/w relative to body weight), followed by having ad lib access to 3% D_2O drinking water.

For the protein and amino acids diet feeding experiment, mice were fed on casein or compositional matched amino acids diet (20% casein, 13% casein + 7% amino acids, 7% casein +13% amino acids, and 20% amino acids as protein/amino acids sources, Table S4) for 2 weeks. Serum was sampled by tail-bleed at 9 am *ad lib*.

Intravenous infusions.—To quantify contribution of circulating nutrients to microbiota metabolism, 9–11-week-old C57BL/6 mice were catheterized in house in the right jugular vein. The mice were infused with carbon or nitrogen-labeled tracer starting at 3:30 pm without any fasting. Infusion rate was 0.1 ul/min/g. Infusion solutions are described in Table

S2A. Overnight (24 h) infusions both started and finished around 9 am. The contribution of circulating nutrient to each metabolite is calculated by the metabolite labeling enrichment normalized to the average tracer serum enrichment throughout 24 hr.

Antibiotics treatment.—To deplete the mouse resident microbiome, an antibiotic drinking water protocol was used. In brief, mice were treated with a cocktail of antibiotics (1 g/L ampicillin, 1 g/L neomycin, 1 g/L metronidazole, and 1 g/L vancomycin) in both their drinking water 14 days. To make the drinking water more palatable, 5% aspartame was added. The effectiveness of antibiotics treatments was verified by observing much lower SCFAs in the feces by LC-MS.

Sample collection.—Systemic blood samples (~6 μl) were collected by tail bleeding. For sampling from tissue-specific draining veins, a mouse was put under anesthesia and different tissue veins were exposed, and blood samples were pulled with an insulin syringe (BD insulin syringes, # SY8290328291) insertion into the vein. Successful isolation of portal vein was confirmed by much higher (> 10x) concentrations of SCFAs and secondary bile acids (deoxycholic acid and lithocholic acid) than systemic vein; hepatic vein was confirmed by much lower secondary bile acids, SCFAs and higher glucose, 3-hydroxybutyrate levels compared to portal vein. Mouse urine was collected from the urinary bladder using a syringe. All serum samples were placed on ice without anticoagulant for 15 min, and centrifuged at 16,000 × g for 15 min at 4 C.

Tissues were harvested by quick dissection and snap freezing (<5 sec) in liquid nitrogen with a pre-cooled Wollenberger clamp; intestinal contents were removed before clamping. For cecal content sampling, the mouse cecum was first removed and cut on the surface, then the cecal content was squeezed out using a tweezer followed by freeze clamping. Whole liver, intestine, and intestinal contents were collected and grounded to homogenous powder. To sample fresh feces, the mouse belly was gently massaged to induce defecation and fresh feces were freeze clamped. For long-term feces collection, a mouse was transferred to a new cage and mouse fecal pellets on the bedding were collected every 1~2 h and freeze clamped. Serum, tissue, and feces samples were kept at −80 °C until further analysis.

16S rRNA gene amplicon sequencing and analysis.—Extraction of Bacterial DNA from cecal or fecal samples was performed using the Power Soil DNA Isolation kit (QIAGEN). A section of the 16S rRNA gene (~250 bp, V4 region) was amplified, and Illumina sequencing libraries were prepared from these amplicons according to a previously published protocol and primers (Caporaso et al., 2012). Libraries were further pooled together at equal molar ratios and sequenced on an Illumina HiSeq 2500 Rapid Flowcell or MiSeq as paired-end reads. These reads were 2×150 bp with an average depth of ~20,000 reads. Also included were 8 bp index reads, following the manufacturer's protocol (Illumina, USA). Pass-Filter reads were generated from raw sequencing reads using Illumina HiSeq Control Software. Samples were de-multiplexed using the index reads. The DADA2 plugin within QIIME2 version 2018.6 was used to inferred Amplicon sequencing variants (ASVs) from the unmerged paired-end sequences (Bolyen et al., 2019; Callahan et al., 2016). The forward reads were trimmed at 150 bp and the reverse reads trimmed at 140 bp, with all other DADA2 as default. Taxonomy was assigned to the resulting ASVs with a naïve Bayes

classifier trained on the Greengenes database version 13.8, with only the target region of the 16S rRNA gene used to train the classifier (Bokulich et al., 2018; McDonald et al., 2012). Downstream analyses were performed MATLAB (Hunter, 2007; McKinney, 2010).

Bacterial culture studies.—For the D_2O experiment, 250 – 1000 μl D_2O was added into the media (5–10 mL, to reach a final enrichment of 5–10%) with either *B. dorei* or *C. sporogenes*, and OD_{600} was recorded at the addition. After every 25–30 min, OD_{600} was recorded and 100–200 μl bacterial solution was taken for metabolomics and proteomics analysis. The newly synthesized fraction of bacteria was calculated by $(OD_{600} - OD_{600,\ 0min})/OD_{600}$.

Bacterial colonization in mice.—Mice were treated with antibiotics in drinking water for 10 days. On day 11, no antibiotics were administered, and mice were gavaged with 250 μl of bacterial consortia consisting of urease-negative bacteria (*B. dorei, C. sporogenes and E. coli*) or a combination of urease-negative and urease-positive bacteria (*B. dorei, C. sporogenes, E. coli, S. aureus and L. reuteri*).

Metabolite extraction.—For serum samples, 3 ul serum was added to 90 ul methanol and incubated on ice for 10 min, followed by centrifugation at 17,000 × g for 10 min at 4°C. The supernatant was transferred to an MS vial until further analysis. For tissues and feces samples, frozen samples were first ground at liquid nitrogen temperature with a cryomill (Restch, Newtown, PA). The resulting tissue powder was extracted with 40:40:20 methanol: acetonitrile: water (40 ul extraction solvent per 1 mg tissue) for 10 min on ice, followed by centrifugation at 17,000 × g for 10 min, the supernatant was transferred to a MS vial until further analysis.

Measurements of metabolites, protein, and polysaccharides.—To measure metabolites in serum, tissue and feces samples, a quadrupole orbitrap mass spectrometer (Q Exactive; Thermo Fisher Scientific) was coupled to a Vanquish UHPLC system (Thermo Fisher Scientific) with electrospray ionization and scan range m/z from 60 to 1000 at 1 Hz, with a 140,000 resolution. LC separation was performed on an XBridge BEH Amide column (2.1×150 mm, 2.5 μm particle size, 130 Å pore size; Waters Corporation) using a gradient of solvent A (95:5 water: acetonitrile with 20 mM of ammonium acetate and 20 mM of ammonium hydroxide, pH 9.45) and solvent B (acetonitrile). Flow rate was 150 μl/min. The LC gradient was: 0 min, 85% B; 2 min, 85% B; 3 min, 80% B; 5 min, 80% B; 6 min, 75% B; 7 min, 75% B; 8 min, 70% B; 9 min, 70% B; 10 min, 50% B; 12 min, 50% B; 13 min, 25% B; 16 min, 25% B; 18 min, 0% B; 23 min, 0% B; 24 min, 85% B; and 30 min, 85% B. Injection volume was 5–10 μl and autosampler temperature was set at 4°C. For cysteine measurement, samples were derivatized before measurement as follows: Serum, cecal content or feces samples were extracted and centrifuged. To the supernatant, 2 mM N-ethylmaleimide was added and incubated at room temperature for 20 min. The resulting mixture was transferred to a MS vial. Derivatized cysteine has a m/z at 245.06015 in negative mode.

To quantify the metabolite concentration in serum and tissue samples, either isotope spike-in or standard spike-in was performed. For isotope spike-in, known concentrations

of isotope-labeled standard were added to the serum or tissues extraction solution, then the concentration was calculated by the ratio of labeled and unlabeled metabolites. When isotope standard is not available, a serially diluted non-labeled standard was added, and a linear fitting between measured total ion count and added concentration of standard was generated. Then, the concentration of endogenous metabolite was determined by the x intercept of the fitting line.

Starch and inulin were measured by acid hydrolysis and LC-MS. In brief, 5–10 mg sample was mixed with 10 μl 2 M hydrochloric acid, and samples were incubated at 80°C for 2 h. After cooling down, the resulting mixture was neutralized with 12 μl saturated sodium bicarbonate, followed with 88 μl 1:1 acetonitrile: methanol solution. After centrifugation at 17,000 × g for 10 min at 4°C, the supernatant was transferred to a MS vial. Inulin and starch concentration in samples was inferred from total ion count of fructose and glucose, respectively.

SCFAs and BCFAs were derivatized and measured by LC-MS. Serum (5 μl) or tissue samples (~10 mg) were added to 100 μl derivatizing reagents containing 12 mM 1-Ethyl-3-(3-dimethylaminopropyl) carbodiimide, 21 mM 3-Nitrophenylhydrazine hydrochloride acid and pyridine (2.4% v/v) in methanol. The reaction was incubated at 4°C for 1 h. Then, the reaction mixture was centrifuged at 17,000 g for 10 min. 20 μl supernatant was quenched with 200 μl 0.5 mM beta-mercaptoethanol in 0.1% formic acid water. After centrifugation at 17,000 g for 10 min, the supernatant was transferred to MS vials until further analysis. The measurement of SCFAs and BCFAs are performed using the same Q Exactive PLUS hybrid quadrupole-orbitrap mass spectrometer with different column and LC setup. LC separation was on Acquity UPLC BEH C18 column (2.1 mm × 100 mm, 1.7 5 μm particle size, 130 Å pore size, Waters, Milford, MA) using a gradient of solvent A (water) and solvent B (methanol). Flow rate was 200 μL/min. The LC gradient was : 0 min, 10% B; 1 min, 10% B; 5 min, 30% B; 11 min 100% B; 14 min, 100% B; 14.5 min 10% B; 22 min 10 % B. Autosampler temperature was 5 °C, column temperature was 60 °C and injection volume was 10 μl. Ion masses for derivatized acetate, propionate, butyrate, iso-butyrate, valeric acid, isovaleric acid, 2-methylbutyrate, 4-methylvaleric acid were 194.0571, 208.0728, 222.0884, 222.0884, 236.1041, 236.1041, 236.1041, 250.1197 in negative mode, respectively.

The ammonia derivatization method was modified from the previous reported Berthelot reaction assay (Spinelli et al., 2017b, 2017a). In brief, 20 mg tissue or 10 μl serum was extracted by using 200 μl 80% methanol. 100 μl of the metabolite extract was mixed with 100 μl. Solution #1 (100 mM Phenol, 50 mg/L sodium nitroprusside) and 100 μl. Solution #2 (0.38 M dibasic sodium phosphate, 125 mM NaOH, 1% sodium hypochlorite, available chlorine 10–15%). The mixture was incubated at 40°C for 30 min. Then, 100 μl reaction solution was mixed with 200 μl methanol to oversaturate the inorganic salt to quench the reaction. The final solution was centrifuged for 30 min. Then the supernatant was loaded to LC-MS for analysis. Ion mass for derivatized ammonia is 198.05605 in negative ion mode.

Protein amino acid composition was measured by acid hydrolysis. Approximately 10 mg of protein was extracted with 400 μl methanol, 200 μl chloroform and 300 μl water, followed

by centrifugation at 20,000 × g for 10 min at 4 °C. The upper layer was removed. The resulting mixture was further extracted with 600 µl methanol twice and supernatant was discarded. The resulting precipitate was dried under nitrogen gas and then hydrolyzed with 250 µl 6 M hydrochloric acid incubated overnight at 115°C. After incubation, the samples were dried under nitrogen gas and reconstituted in 1 mL methanol, and the supernatant was transferred to a MS vial for analysis. Amino acid composition of the proteins used in the study are shown in Figure S4F, and such differences in protein amino acid composition do not correlate with the quantified dietary protein contribution to cecal amino acids (Figure S4G).

Proteomics sample preparation.—Proteomics samples were prepared mostly as previously described (Gupta et al., 2018; Wühr et al., 2014). Mouse cecal samples (10 mg each) were dissolved in 400 µl lysis buffer (6M guanidium chloride, 2% cetrimonium bromide, 5 mM dithiothreitol, 50 mM (4-(2-hydroxyethyl)-1-piperazineethanesulfonic acid) (HEPES), pH 7.2). Then the sample mixture was put on ice and sonicated for 10 cycles (30 s on and 30 s off cycle, amplitude 50%) by a sonicator (Qsonica), followed by centrifugation at 20,000 × g for 20 min at 4 °C. The supernatant was taken and alkylated with 20 mM N-ethylmaleimide for 20 min at room temperature, 5 mM dithiothreitol was added to quench the excessive alkylating reagents. Proteins were purified by methanol-chloroform precipitation. The dried protein pellet was resuspended in 10 mM EPPS (N-(2-Hydroxyethyl) piperazine-N'-(3-propanesulfonic acid)) at pH 8.5 with 6 M guanidine hydrochloride. Samples were heated at 60°C for 15 min and protein concentration was determined by BCA assay (Pierce BCA Protein Assay Kit, Thermo Scientific). The protein mixture (30~50 µg) was diluted with 10 mM EPPS pH 8.5 to 2 M GuaCl and digested with 10 ng/µL LysC (Wako) at room temperature overnight. Samples were further diluted to 0.5 M GuaCl with 10 M EPPS pH 8.5 and digested with an additional 10 ng/µL LysC and 20 ng/µL sequencing grade Trypsin (Promega) at 37°C for 16 h. Samples were desalted using a SepPak cartridges (Waters) and then vacuum-dried and resuspended in 1% formic acid before mass spectrometry analysis.

Proteomics peptide measurement.—Samples were analyzed on an EASY-nLC 1200 (Thermo Fisher Scientific) HPLC coupled to an Orbitrap Fusion Lumos mass spectrometer (Thermo Fisher Scientific) with Tune version 3.3. Peptides were separated on an Aurora Series emitter column (25 cm × 75 µm ID, 1.6 µm C18) (Ionopticks, Australia) and held at 60°C during separation using an in-house built column oven over 180 min, applying nonlinear acetonitrile gradients at a constant flow rate of 350 nL/min. The Fusion Lumos was operated in data dependent mode. The survey scan was performed at a resolution setting of 120k in orbitrap, followed by MS2 duty cycle of 1.5 s. The normalized collision energy for CID MS2 experiments was set to 30%.

Solvent A consisted of 2% DMSO (LC-MS-grade, Life Technologies), 0.125% formic acid (98%+, TCI America) in water (LC-MS-grade, OmniSolv, VWR), solvent B of 80% acetonitrile (LC-MS-grade, OmniSolv, Millipore Sigma), 2% DMSO and 0.125% formic acid in water. The following 120 min-gradient with percentage of solvent B were applied at a constant flow rate of 350 nL/min after thorough equilibration of the column to 0% B:

0% – 6% in 5 min; 6 – 25% in 160 min; 25% –100% in 10 min; 100% for 5 min. For electrospray ionization, 2.6 kV were applied between minutes 1 and 113 (or minutes 1 and 83 for fractionated samples) of the gradient through the column. To avoid carry-over of peptides, 2,2,2-trifluoroethanol (>99% Reagent plus, Millipore Sigma) was injected in a 30 min wash between each sample.

Proteomics data analysis.—The data was analyzed using GFY software licensed from Harvard (Nusinow et al., 2020). Thermo Fisher Scientific. raw files were converted to mzXML using ReAdW.exe. MS2 spectra assignment was performed using the SEQUEST algorithm v.28 (rev. 12) by searching the data against the combined reference proteomes for *Mus Musculus*, *Bos Taurus*, and all the abundant bacterial families detected in 16S rRNA gene amplicon sequencing (*Bacteroidaceae, Porphyromonadaceae, Prevotellaceae, Rikenellaceae, Muribaculaceae, Lachnospiraceae, Ruminococcaceae, Erysipelotrichaceae, Oscillospiraceae, Clostridiaceae, Eubacteriaceae, Lactobacillaceae* and *Verrucomicrobiaceae*) acquired from Uniprot on Jan 2021 (SwissProt + Trembl) along with common contaminants such as human keratins and trypsin. The target-decoy strategy was used to construct a second database of reverse sequences that were used to estimate the peptide false discovery rate (Elias and Gygi, 2007). A 20-ppm precursor ion tolerance with the requirement that both N- and C- terminal peptide ends are consistent with the protease specificities of LysC and Trypsin was used for SEQUEST searches, two missed cleavage was allowed. NEM was set as a static modification of cysteine residues (+125.047679 Da). An MS2 spectral assignment false discovery rate of 0.5% was achieved by applying the target decoy database search strategy. Linear Discriminant analysis was used for filtering with the following features: SEQUEST parameters XCorr and unique ΔXCorr, absolute peptide ion mass accuracy, peptide length and charge state. Forward peptides within three standard deviations of the theoretical m/z of the precursor were used as positive training set. All reverse peptides were used as negative training set. Linear Discriminant scores were used to sort peptides with at least seven residues and to filter with the desired cutoff. Furthermore, we performed a filtering step on the protein level by the “picked” protein FDR approach (Savitski et al., 2015). Protein redundancy was removed by assigning peptides to the minimal number of proteins which can explain all observed peptide, with above-described filtering criteria.

To quantify the intensities of all the isotopic peaks of the peptides, we used raw intensity. Missed cleavage peptides (more than one K or R in the peptide) and low signal to FT-noise peptides (M_0 S/N < 20) were removed. Peptide phylogenetic assignment was performed using Unipept 4.0 (Gurdeep Singh et al., 2019), ‘Equate I and L’ and ‘Advanced missed cleavage handling’ were not selected. Only peptides that are specific at a genus level were used for further analysis.

Quantification of newly-synthesized fraction of peptide.—To determine the newly synthesized fraction of a bacterial peptide in D_2O drinking water experiment, we first measured the cecal content free amino acids deuterium labeling pattern using metabolomics. Then, for each peptide, we simulated the expected isotope envelope pattern if the peptide were old, i.e., unlabeled with deuterium (I_{old}), versus if it were newly synthesized by taking

up free amino acids from the cecal content (I_{new}). I_{old} was calculated based on the peptide's molecular formula and ^{13}C, ^{15}N, ^{2}H, ^{17}O, ^{18}O, ^{32}S, ^{33}S and ^{36}S natural abundance. I_{new} was calculated based on the peptide's sequence and experimentally observed labeling of the corresponding cecal free amino acids (after natural isotope correction), and the natural isotope abundance of the unlabeled atoms in the peptide's formula. The simulation of expected peptide isotope distribution and fitting was performed using a MATLAB code: https://github.com/xxing9703/pepMID_simul. Exact mass isotopic peaks with appreciable abundances were bundled by nominal mass into fraction M+0, M+1, …M+n, constituting the final simulated spectrum. A least square fit was used to find the scalar θ that best fit the measured peptide isotopic distribution ($I_{measured}$) to a linear combination of I_{old} and I_{new}:

$$I_{measured} = I_{old} \times (1 - \theta) + I_{new} \times \theta$$

The root mean square error was determined for each peptide fitting, and any fitting with a root mean square error > 1% was removed. For genus-level turnover quantification, only genera with more than two measurements were kept in the analysis, with the median value across peptides reported.

Quantification of contribution of labeled nutrient to peptide.—To determine the contribution of a ^{13}C- or ^{15}N-labeled nutrient to a bacterial peptide, similar to the above approach, we first measured the cecal content free amino acids ^{13}C- or ^{15}N-labeling using metabolomics. Then, for each peptide, we simulated the expected isotope envelope pattern if the peptide were unlabeled ($I_{unlabeled}$) versus if it were synthesized from free cecal amino acids (I_{free}). A scalar γ (analogous to θ above) can then be determined by fitting the measured peptide isotope distribution ($I_{measured}$) to a linear combination of $I_{unlabeled}$ and I_{free}. Note that γ will exceed 1 when a bacterial genus uses a particular nutrient in excess of that nutrient contribution's to cecal free amino acids. Because the ^{13}C- and ^{15}N-labeling patterns are simpler than the D_2O labeling patterns, in lieu of carrying out this fitting, we instead determined γ (with the same conceptual and mathematical meaning) using simple algebraic equations.

Specifically, we measured γ for each peptide as follows:

$$\gamma = \frac{\varphi_{measured} - \varphi_{unlabeled}}{\varphi_{free} - \varphi_{unlabeled}}$$

where (with the exception of ^{13}C-protein feeding data, discussed immediately below) φ is the average number of extra neutrons in a given peptide (or simulated peptide), relative to the M+0 form. This was calculated based on the experimentally observed (or simulated, as above) fraction of M+0, M+1, M+2, and M+3, which account for > 90% of the isotopes for each peptide (with more heavily labeled forms too low abundance and noisy to contribute productively to the measurements):

$$\varphi = \frac{\sum_{i=0}^{3} i \cdot M_i}{\sum_{i=0}^{3} M_i}$$

For the ^{13}C-protein feeding experiments, the most readily detected labeled forms involve incorporation of a single midsized U-^{13}C-amino acid, which manifests as M+5 or M+6 peptide labeling. Other isotopic forms were sufficiently noisier, as to render their inclusion unhelpful. Accordingly, we calculated γ based on φ':

$$\varphi' = \frac{M_5 + M_6}{M_0 + M_5 + M_6}$$

The above equations give nearly identical values for γ as fitting (as done to determine θ).

For genus-level measurements of feedstock contributions, only genera with more than 3 peptides measured per mouse was kept in the analysis, with the median value across peptides reported as γ_{genus}. Only genera that were consistently detected in proteomics, and the family of that genera detected (> 0.5%) in 16S rRNA gene amplicon sequencing were analyzed. The product of γ_{genus} and the contribution of each nutrient to cecal free amino acids ($L_{AA\_avg \leftarrow nutrient}$) was used to determine the contribution of each nutrient to bacterial genus ($f_{genus \leftarrow nutrient}$):

$$f_{genus \leftarrow nutrient} = \gamma_{genus} \times L_{AA\_avg \leftarrow nutrient}$$

where the contribution of each nutrient to bacterial protein pool ($L_{AA\_avg \leftarrow Nutrient}$) was calculated as the average labeling across amino acids, weighted based on their abundance in that genus' protein and corrected for fraction of the nutrient interest labeled (T):

$$L_{AA\_avg \leftarrow nutrient} = \sum f_{Cecal\_AA \leftarrow nutrient} \times w\%_{AA,\, bacteria} / T$$

with $w\%_{AA,bacteria}$ taken from literature (Purser and Buechler, 1966).

Quantification and statistical analysis.—A two-tailed, unpaired student's t-test was used to calculate P values, with $P<0.05$ used to determine statistical significance.

Supplementary Material

Refer to Web version on PubMed Central for supplementary material.

ACKNOWLEDGEMENTS.

This work is supported by the NIH Pioneer award IDP1DK113643 (J.D.R.), Stand Up to Cancer Convergence Award 3.14.16 probing the cancer-microbiome connection (J.D.R.), Ludwig Cancer Research (J.D.R.), NIH grant R35GM128813 (M.W.), Princeton Catalysis Initiative (M.W.), Eric and Wendy Schmidt Transformative Technology Fund (M.W), and the Pew Biomedical Scholars Program (M.S.D). M.G. is funded by Harold W. Dodds Fellowship. F.C.K is funded by EMBO ALTF 601-2018. J.G.L. is funded by a National Science Foundation Graduate Research Fellowship (2017249408). Y.-C.J.L. is funded by the High Meadows Environmental Institute at Princeton

University through the generous support of the William Clay Ford, Jr. ‘79 and Lisa Vanderzee Ford ‘82 Graduate Fellowship fund and by a training grant from the National Institute of General Medicine Sciences (T32GM007388). M.D.N. is supported by NIH 5T32CA257957. We thank Sheng Hui, Michel Nofal, Yihui Shen, Lingfan Liang, Won Dong Lee and other Rabinowitz lab members for the input and advice. We thank Seema Chatterjee for the assistance with DNA extraction. We thank Wei Wang and the Lewis Sigler Institute sequencing core facility for assistance with HT sequencing.

References

Albenberg L, Esipova TV, Judge CP, Bittinger K, Chen J, Laughlin A, Grunberg S, Baldassano RN, Lewis JD, Li H, Thom SR, Bushman FD, Vinogradov SA, Wu GD, 2014. Correlation Between Intraluminal Oxygen Gradient and Radial Partitioning of Intestinal Microbiota. Gastroenterology 147, 1055–1063.e8. 10.1053/j.gastro.2014.07.020 [PubMed: 25046162]

Arab JP, Karpen SJ, Dawson PA, Arrese M, Trauner M, 2017. Bile acids and nonalcoholic fatty liver disease: Molecular insights and therapeutic perspectives. Hepatol. Baltim. Md 65, 350–362. 10.1002/hep.28709

Bartman CR, TeSlaa T, Rabinowitz JD, 2021. Quantitative flux analysis in mammals. Nat. Metab 3, 896–908. 10.1038/s42255-021-00419-2 [PubMed: 34211182]

Batani G, Bayer K, Böge J, Hentschel U, Thomas T, 2019. Fluorescence in situ hybridization (FISH) and cell sorting of living bacteria. Sci. Rep 9, 18618. 10.1038/s41598-019-55049-2 [PubMed: 31819112]

Berry D, Mader E, Lee TK, Woebken D, Wang Y, Zhu D, Palatinszky M, Schintlmeister A, Schmid MC, Hanson BT, Shterzer N, Mizrahi I, Rauch I, Decker T, Bocklitz T, Popp J, Gibson CM, Fowler PW, Huang WE, Wagner M, 2015. Tracking heavy water (D2O) incorporation for identifying and sorting active microbial cells. Proc. Natl. Acad. Sci 112, E194–E203. 10.1073/pnas.1420406112 [PubMed: 25550518]

Berry D, Stecher B, Schintlmeister A, Reichert J, Brugiroux S, Wild B, Wanek W, Richter A, Rauch I, Decker T, Loy A, Wagner M, 2013. Host-compound foraging by intestinal microbiota revealed by single-cell stable isotope probing. Proc. Natl. Acad. Sci 110, 4720–4725. 10.1073/pnas.1219247110 [PubMed: 23487774]

Bokulich NA, Kaehler BD, Rideout JR, Dillon M, Bolyen E, Knight R, Huttley GA, Gregory Caporaso J, 2018. Optimizing taxonomic classification of marker-gene amplicon sequences with QIIME 2’s q2-feature-classifier plugin. Microbiome 6, 90. 10.1186/s40168-018-0470-z [PubMed: 29773078]

Bolyen E, Rideout JR, Dillon MR, Bokulich NA, Abnet CC, Al-Ghalith GA, Alexander H, Alm EJ, Arumugam M, Asnicar F, Bai Y, Bisanz JE, Bittinger K, Brejnrod A, Brislawn CJ, Brown CT, Callahan BJ, Caraballo-Rodríguez AM, Chase J, Cope EK, Da Silva R, Diener C, Dorrestein PC, Douglas GM, Durall DM, Duvallet C, Edwardson CF, Ernst M, Estaki M, Fouquier J, Gauglitz JM, Gibbons SM, Gibson DL, Gonzalez A, Gorlick K, Guo J, Hillmann B, Holmes S, Holste H, Huttenhower C, Huttley GA, Janssen S, Jarmusch AK, Jiang L, Kaehler BD, Kang KB, Keefe CR, Keim P, Kelley ST, Knights D, Koester I, Kosciolek T, Kreps J, Langille MGI, Lee J, Ley R, Liu Y-X, Loftfield E, Lozupone C, Maher M, Marotz C, Martin BD, McDonald D, McIver LJ, Melnik AV, Metcalf JL, Morgan SC, Morton JT, Naimey AT, Navas-Molina JA, Nothias LF, Orchanian SB, Pearson T, Peoples SL, Petras D, Preuss ML, Pruesse E, Rasmussen LB, Rivers A, Robeson MS, Rosenthal P, Segata N, Shaffer M, Shiffer A, Sinha R, Song SJ, Spear JR, Swafford AD, Thompson LR, Torres PJ, Trinh P, Tripathi A, Turnbaugh PJ, Ul-Hasan S, van der Hooft JJJ, Vargas F, Vázquez-Baeza Y, Vogtmann E, von Hippel M, Walters W, Wan Y, Wang M, Warren J, Weber KC, Williamson CHD, Willis AD, Xu ZZ, Zaneveld JR, Zhang Y, Zhu Q, Knight R, Caporaso JG, 2019. Reproducible, interactive, scalable and extensible microbiome data science using QIIME 2. Nat. Biotechnol 37, 852–857. 10.1038/s41587-019-0209-9 [PubMed: 31341288]

Callahan BJ, McMurdie PJ, Rosen MJ, Han AW, Johnson AJA, Holmes SP, 2016. DADA2: High-resolution sample inference from Illumina amplicon data. Nat. Methods 13, 581–583. 10.1038/nmeth.3869 [PubMed: 27214047]

Campbell C, McKenney PT, Konstantinovsky D, Isaeva OI, Schizas M, Verter J, Mai C, Jin W-B, Guo C-J, Violante S, Ramos RJ, Cross JR, Kadaveru K, Hambor J, Rudensky AY, 2020. Bacterial metabolism of bile acids promotes generation of peripheral regulatory T cells. Nature 1–5. 10.1038/s41586-020-2193-0

Caporaso JG, Lauber CL, Walters WA, Berg-Lyons D, Huntley J, Fierer N, Owens SM, Betley J, Fraser L, Bauer M, Gormley N, Gilbert JA, Smith G, Knight R, 2012. Ultra-high-throughput microbial community analysis on the Illumina HiSeq and MiSeq platforms. ISME J. 6, 1621–1624. 10.1038/ismej.2012.8 [PubMed: 22402401]

Dalile B, Oudenhove LV, Vervliet B, Verbeke K, 2019. The role of short-chain fatty acids in microbiota–gut–brain communication. Nat. Rev. Gastroenterol. Hepatol 1. 10.1038/s41575-019-0157-3

David LA, Maurice CF, Carmody RN, Gootenberg DB, Button JE, Wolfe BE, Ling AV, Devlin AS, Varma Y, Fischbach MA, Biddinger SB, Dutton RJ, Turnbaugh PJ, 2014. Diet rapidly and reproducibly alters the human gut microbiome. Nature 505, 559–563. 10.1038/nature12820 [PubMed: 24336217]

De Vadder F, Kovatcheva-Datchary P, Goncalves D, Vinera J, Zitoun C, Duchampt A, Bäckhed F, Mithieux G, 2014. Microbiota-generated metabolites promote metabolic benefits via gut-brain neural circuits. Cell 156, 84–96. 10.1016/j.cell.2013.12.016 [PubMed: 24412651]

Desai MS, Seekatz AM, Koropatkin NM, Kamada N, Hickey CA, Wolter M, Pudlo NA, Kitamoto S, Terrapon N, Muller A, Young VB, Henrissat B, Wilmes P, Stappenbeck TS, Núñez G, Martens EC, 2016. A Dietary Fiber-Deprived Gut Microbiota Degrades the Colonic Mucus Barrier and Enhances Pathogen Susceptibility. Cell 167, 1339–1353.e21. 10.1016/j.cell.2016.10.043 [PubMed: 27863247]

Elias JE, Gygi SP, 2007. Target-decoy search strategy for increased confidence in large-scale protein identifications by mass spectrometry. Nat. Methods 4, 207–214. 10.1038/nmeth1019 [PubMed: 17327847]

Faubert B, Li KY, Cai L, Hensley CT, Kim J, Zacharias LG, Yang C, Do QN, Doucette S, Burguete D, Li H, Huet G, Yuan Q, Wigal T, Butt Y, Ni M, Torrealba J, Oliver D, Lenkinski RE, Malloy CR, Wachsmann JW, Young JD, Kernstine K, DeBerardinis RJ, 2017. Lactate Metabolism in Human Lung Tumors. Cell 171, 358–371.e9. 10.1016/j.cell.2017.09.019 [PubMed: 28985563]

Fernández-García J, Altea-Manzano P, Pranzini E, Fendt S-M, 2020. Stable Isotopes for Tracing Mammalian-Cell Metabolism In Vivo. Trends Biochem. Sci 45, 185–201. 10.1016/j.tibs.2019.12.002 [PubMed: 31955965]

Funabashi M, Grove TL, Wang M, Varma Y, McFadden ME, Brown LC, Guo C, Higginbottom S, Almo SC, Fischbach MA, 2020. A metabolic pathway for bile acid dehydroxylation by the gut microbiome. Nature 582, 566–570. 10.1038/s41586-020-2396-4 [PubMed: 32555455]

Garrett WS, 2015. Cancer and the microbiota. Science 348, 80–86. 10.1126/science.aaa4972 [PubMed: 25838377]

Gupta M, Sonnett M, Ryazanova L, Presler M, Wühr M, 2018. Quantitative Proteomics of Xenopus Embryos I, Sample Preparation, in: Vleminckx K. (Ed.), Xenopus: Methods and Protocols, Methods in Molecular Biology. Springer, New York, NY, pp. 175–194. 10.1007/978-1-4939-8784-9_13

Gurdeep Singh R, Tanca A, Palomba A, Van der Jeugt F, Verschaffelt P, Uzzau S, Martens L, Dawyndt P, Mesuere B, 2019. Unipept 4.0: Functional Analysis of Metaproteome Data. J. Proteome Res 18, 606–615. 10.1021/acs.jproteome.8b00716 [PubMed: 30465426]

Halestrap AP, Price NT, 1999. The proton-linked monocarboxylate transporter (MCT) family: structure, function and regulation. Biochem. J 343, 281–299. [PubMed: 10510291]

Han S, Van Treuren W, Fischer CR, Merrill BD, DeFelice BC, Sanchez JM, Higginbottom SK, Guthrie L, Fall LA, Dodd D, Fischbach MA, Sonnenburg JL, 2021. A metabolomics pipeline for the mechanistic interrogation of the gut microbiome. Nature 595, 415–420. 10.1038/s41586-021-03707-9 [PubMed: 34262212]

Hang S, Paik D, Yao L, Kim E, Trinath J, Lu J, Ha S, Nelson BN, Kelly SP, Wu L, Zheng Y, Longman RS, Rastinejad F, Devlin AS, Krout MR, Fischbach MA, Littman DR, Huh JR, 2019. Bile acid metabolites control T H 17 and T reg cell differentiation. Nature 576, 143–148. 10.1038/s41586-019-1785-z [PubMed: 31776512]

Holmes AJ, Chew YV, Colakoglu F, Cliff JB, Klaassens E, Read MN, Solon-Biet SM, McMahon AC, Cogger VC, Ruohonen K, Raubenheimer D, Le Couteur DG, Simpson SJ, 2017. Diet-Microbiome Interactions in Health Are Controlled by Intestinal Nitrogen Source Constraints. Cell Metab. 25, 140–151. 10.1016/j.cmet.2016.10.021 [PubMed: 27889387]

Holmes WE, Angel TE, Li KW, Hellerstein MK, 2015. Chapter Seven - Dynamic Proteomics: In Vivo Proteome-Wide Measurement of Protein Kinetics Using Metabolic Labeling, in: Metallo CM (Ed.), Methods in Enzymology, Metabolic Analysis Using Stable Isotopes. Academic Press, pp. 219–276. 10.1016/bs.mie.2015.05.018

Hui S, Ghergurovich JM, Morscher RJ, Jang C, Teng X, Lu W, Esparza LA, Reya T, Zhan L, Guo JY, White E, Rabinowitz JD, 2017. Glucose feeds the TCA cycle via circulating lactate. Nature 551, 115–118. 10.1038/nature24057 [PubMed: 29045397]

Hunter JD, 2007. Matplotlib: A 2D Graphics Environment. Comput. Sci. Eng 9, 90–95. 10.1109/MCSE.2007.55

Jang C, Hui S, Lu W, Cowan AJ, Morscher RJ, Lee G, Liu W, Tesz GJ, Birnbaum MJ, Rabinowitz JD, 2018. The Small Intestine Converts Dietary Fructose into Glucose and Organic Acids. Cell Metab. 27, 351–361.e3. 10.1016/j.cmet.2017.12.016 [PubMed: 29414685]

Jang C, Hui S, Zeng X, Cowan AJ, Wang L, Chen L, Morscher RJ, Reyes J, Frezza C, Hwang HY, Imai A, Saito Y, Okamoto K, Vaspoli C, Kasprenski L, Zsido GA, Gorman JH, Gorman RC, Rabinowitz JD, 2019. Metabolite Exchange between Mammalian Organs Quantified in Pigs. Cell Metab. 30, 594–606.e3. 10.1016/j.cmet.2019.06.002 [PubMed: 31257152]

Koh A, Molinaro A, Ståhlman M, Khan MT, Schmidt C, Mannerås-Holm L, Wu H, Carreras A, Jeong H, Olofsson LE, Bergh P-O, Gerdes V, Hartstra A, Brauw M. de, Perkins R, Nieuwdorp M, Bergström G, Bäckhed F, 2018. Microbially Produced Imidazole Propionate Impairs Insulin Signaling through mTORC1. Cell 175, 947–961.e17. 10.1016/j.cell.2018.09.055 [PubMed: 30401435]

Koh A, Vadder FD, Kovatcheva-Datchary P, Bäckhed F, 2016. From Dietary Fiber to Host Physiology: Short-Chain Fatty Acids as Key Bacterial Metabolites. Cell 165, 1332–1345. 10.1016/j.cell.2016.05.041 [PubMed: 27259147]

Lai Y, Liu C-W, Yang Y, Hsiao Y-C, Ru H, Lu K, 2021. High-coverage metabolomics uncovers microbiota-driven biochemical landscape of interorgan transport and gut-brain communication in mice. Nat. Commun 12, 6000. 10.1038/s41467-021-26209-8 [PubMed: 34667167]

Li H, Limenitakis JP, Fuhrer T, Geuking MB, Lawson MA, Wyss M, Brugiroux S, Keller I, Macpherson JA, Rupp S, Stolp B, Stein JV, Stecher B, Sauer U, McCoy KD, Macpherson AJ, 2015. The outer mucus layer hosts a distinct intestinal microbial niche. Nat. Commun 6, 8292. 10.1038/ncomms9292 [PubMed: 26392213]

Liu Z, Liu H-Y, Zhou H, Zhan Q, Lai W, Zeng Q, Ren H, Xu D, 2017. Moderate-Intensity Exercise Affects Gut Microbiome Composition and Influences Cardiac Function in Myocardial Infarction Mice. Front. Microbiol 8. 10.3389/fmicb.2017.01687

Lund PJ, Gates LA, Leboeuf M, Smith SA, Chau L, Friedman ES, Lopes M, Saiman Y, Kim MS, Petucci C, Allis CD, Wu GD, Garcia BA, 2021. Stable Isotope Tracing in vivo Reveals A Metabolic Bridge Linking the Microbiota to Host Histone Acetylation. bioRxiv 2021.07.05.450926. 10.1101/2021.07.05.450926

Madsen L, Myrmel LS, Fjære E, Liaset B, Kristiansen K, 2017. Links between Dietary Protein Sources, the Gut Microbiota, and Obesity. Front. Physiol 8, 1047. 10.3389/fphys.2017.01047 [PubMed: 29311977]

Mager LF, Burkhard R, Pett N, Cooke NCA, Brown K, Ramay H, Paik S, Stagg J, Groves RA, Gallo M, Lewis IA, Geuking MB, McCoy KD, 2020. Microbiome-derived inosine modulates response to checkpoint inhibitor immunotherapy. Science. 10.1126/science.abc3421

McCabe BJ, Previs SF, 2004. Using isotope tracers to study metabolism: application in mouse models. Metab. Eng 6, 25–35. 10.1016/j.ymben.2003.09.003 [PubMed: 14734253]

McDonald D, Price MN, Goodrich J, Nawrocki EP, DeSantis TZ, Probst A, Andersen GL, Knight R, Hugenholtz P, 2012. An improved Greengenes taxonomy with explicit ranks for ecological and evolutionary analyses of bacteria and archaea. ISME J. 6, 610–618. 10.1038/ismej.2011.139 [PubMed: 22134646]

McKinney W, 2010. Data Structures for Statistical Computing in Python. Proc. 9th Python Sci. Conf 56–61. 10.25080/Majora-92bf1922-00a

Mora D, Arioli S, 2014. Microbial Urease in Health and Disease. PLOS Pathog. 10, e1004472. 10.1371/journal.ppat.1004472 [PubMed: 25501953]

Munukka E, Ahtiainen JP, Puigbó P, Jalkanen S, Pahkala K, Keskitalo A, Kujala UM, Pietilä S, Hollmén M, Elo L, Huovinen P, D'Auria G, Pekkala S, 2018. Six-Week Endurance Exercise Alters Gut Metagenome That Is not Reflected in Systemic Metabolism in Over-weight Women. Front. Microbiol 9. 10.3389/fmicb.2018.02323

Nemet I, Saha PP, Gupta N, Zhu W, Romano KA, Skye SM, Cajka T, Mohan ML, Li L, Wu Y, Funabashi M, Ramer-Tait AE, Prasad SVN, Fiehn O, Rey FE, Tang WHW, Fischbach MA, DiDonato JA, Hazen SL, 2020. A Cardiovascular Disease-Linked Gut Microbial Metabolite Acts via Adrenergic Receptors. Cell 180, 862–877.e22. 10.1016/j.cell.2020.02.016 [PubMed: 32142679]

Ni J, Shen T-CD, Chen EZ, Bittinger K, Bailey A, Roggiani M, Sirota-Madi A, Friedman ES, Chau L, Lin A, Nissim I, Scott J, Lauder A, Hoffmann C, Rivas G, Albenberg L, Baldassano RN, Braun J, Xavier RJ, Clish CB, Yudkoff M, Li H, Goulian M, Bushman FD, Lewis JD, Wu GD, 2017. A role for bacterial urease in gut dysbiosis and Crohn's disease. Sci. Transl. Med 9. 10.1126/scitranslmed.aah6888

Nusinow DP, Szpyt J, Ghandi M, Rose CM, McDonald ER, Kalocsay M, Jané-Valbuena J, Gelfand E, Schweppe DK, Jedrychowski M, Golji J, Porter DA, Rejtar T, Wang YK, Kryukov GV, Stegmeier F, Erickson BK, Garraway LA, Sellers WR, Gygi SP, 2020. Quantitative Proteomics of the Cancer Cell Line Encyclopedia. Cell 180, 387–402.e16. 10.1016/j.cell.2019.12.023 [PubMed: 31978347]

Oberbach A, Haange S-B, Schlichting N, Heinrich M, Lehmann S, Till H, Hugenholtz F, Kullnick Y, Smidt H, Frank K, Seifert J, Jehmlich N, von Bergen M, 2017. Metabolic in Vivo Labeling Highlights Differences of Metabolically Active Microbes from the Mucosal Gastrointestinal Microbiome between High-Fat and Normal Chow Diet. J. Proteome Res 16, 1593–1604. 10.1021/acs.jproteome.6b00973 [PubMed: 28252966]

O'Brien JJ, Narayan V, Wong Y, Seitzer P, Sandoval CM, Haste N, Smith M, Rad R, Gaun A, Baker A, Kukurugya M, Martin-McNulty B, Zhang C, Kolumam G, Sidrauski C, Jojic V, McAllister F, Bennett B, Buffenstein R, 2020. Precise Estimation of In Vivo Protein Turnover Rates. bioRxiv 2020.11.10.377440. 10.1101/2020.11.10.377440

Purser DB, Buechler SM, 1966. Amino Acid Composition of Rumen Organisms. J. Dairy Sci 49, 81–84. 10.3168/jds.S0022-0302(66)87791-3 [PubMed: 5908803]

Qin J, Li R, Raes J, Arumugam M, Burgdorf KS, Manichanh C, Nielsen T, Pons N, Levenez F, Yamada T, Mende DR, Li J, Xu J, Li Shaochuan Li D, Cao J, Wang B, Liang H, Zheng H, Xie Y, Tap J, Lepage P, Bertalan M, Batto J-M, Hansen T, Le Paslier D, Linneberg A, Nielsen HB, Pelletier E, Renault P, Sicheritz-Ponten T, Turner K, Zhu H, Yu C, Li Shengting, Jian M, Zhou Y, Li Y, Zhang X, Li Songgang, Qin N, Yang H, Wang Jian, Brunak S, Doré J, Guarner F, Kristiansen K, Pedersen O, Parkhill J, Weissenbach J, Bork P, Ehrlich SD, Wang, Jun, 2010. A human gut microbial gene catalogue established by metagenomic sequencing. Nature 464, 59–65. 10.1038/nature08821 [PubMed: 20203603]

Quinn RA, Melnik AV, Vrbanac A, Fu T, Patras KA, Christy MP, Bodai Z, Belda-Ferre P, Tripathi A, Chung LK, Downes M, Welch RD, Quinn M, Humphrey G, Panitchpakdi M, Weldon KC, Aksenov A, da Silva R, Avila-Pacheco J, Clish C, Bae S, Mallick H, Franzosa EA, Lloyd-Price J, Bussell R, Thron T, Nelson AT, Wang M, Leszczynski E, Vargas F, Gauglitz JM, Meehan MJ, Gentry E, Arthur TD, Komor AC, Poulsen O, Boland BS, Chang JT, Sandborn WJ, Lim M, Garg N, Lumeng JC, Xavier RJ, Kazmierczak BI, Jain R, Egan M, Rhee KE, Ferguson D, Raffatellu M, Vlamakis H, Haddad GG, Siegel D, Huttenhower C, Mazmanian SK, Evans RM, Nizet V, Knight R, Dorrestein PC, 2020. Global chemical effects of the microbiome include new bile-acid conjugations. Nature 579, 123–129. 10.1038/s41586-020-2047-9 [PubMed: 32103176]

Reese AT, Pereira FC, Schintlmeister A, Berry D, Wagner M, Hale LP, Wu A, Jiang S, Durand HK, Zhou X, Premont RT, Diehl AM, O'Connell TM, Alberts SC, Kartzinel TR, Pringle RM, Dunn RR, Wright JP, David LA, 2018. Microbial nitrogen limitation in the mammalian large intestine. Nat. Microbiol 3, 1441–1450. 10.1038/s41564-018-0267-7 [PubMed: 30374168]

Ridlon JM, Kang DJ, Hylemon PB, Bajaj JS, 2014. Bile Acids and the Gut Microbiome. Curr. Opin. Gastroenterol 30, 332–338. 10.1097/MOG.0000000000000057 [PubMed: 24625896]

Savitski MM, Wilhelm M, Hahne H, Kuster B, Bantscheff M, 2015. A Scalable Approach for Protein False Discovery Rate Estimation in Large Proteomic Data Sets. Mol. Cell. Proteomics MCP 14, 2394–2404. 10.1074/mcp.M114.046995 [PubMed: 25987413]

Scheiman J, Luber JM, Chavkin TA, MacDonald T, Tung A, Pham L-D, Wibowo MC, Wurth RC, Punthambaker S, Tierney BT, Yang Z, Hattab MW, Avila-Pacheco J, Clish CB, Lessard S, Church GM, Kostic AD, 2019. Meta-omics analysis of elite athletes identifies a performance-enhancing microbe that functions via lactate metabolism. Nat. Med 1. 10.1038/s41591-019-0485-4

Sicard J-F, Le Bihan G, Vogeleer P, Jacques M, Harel J, 2017. Interactions of Intestinal Bacteria with Components of the Intestinal Mucus. Front. Cell. Infect. Microbiol 7. 10.3389/fcimb.2017.00387

Spinelli JB, Kelley LP, Haigis MC, 2017a. An LC-MS Approach to Quantitative Measurement of Ammonia Isotopologues. Sci. Rep 7, 10304. 10.1038/s41598-017-09993-6 [PubMed: 28871132]

Spinelli JB, Yoon H, Ringel AE, Jeanfavre S, Clish CB, Haigis MC, 2017b. Metabolic recycling of ammonia via glutamate dehydrogenase supports breast cancer biomass. Science 358, 941–946. 10.1126/science.aam9305 [PubMed: 29025995]

Tang WHW, Wang Z, Levison BS, Koeth RA, Britt EB, Fu X, Wu Y, Hazen SL, 2013. Intestinal Microbial Metabolism of Phosphatidylcholine and Cardiovascular Risk [WWW Document]. http://dx.doi.org/10.1056/NEJMoa1109400. 10.1056/NEJMoa1109400

Ullrich KJ, Rumrich G, Klöss S, 1982. Reabsorption of monocarboxylic acids in the proximal tubule of the rat kidney. II. Specificity for aliphatic compounds. Pflüg. Arch. Eur. J. Physiol 395, 220–226. 10.1007/BF00584813

Wali JA, Milner AJ, Luk AWS, Pulpitel TJ, Dodgson T, Facey HJW, Wahl D, Kebede MA, Senior AM, Sullivan MA, Brandon AE, Yau B, Lockwood GP, Koay YC, Ribeiro R, Solon-Biet SM, Bell-Anderson KS, O'Sullivan JF, Macia L, Forbes JM, Cooney GJ, Cogger VC, Holmes A, Raubenheimer D, Le Couteur DG, Simpson SJ, 2021. Impact of dietary carbohydrate type and protein–carbohydrate interaction on metabolic health. Nat. Metab 1–19. 10.1038/s42255-021-00393-9 [PubMed: 33483718]

Wang Z, Klipfell E, Bennett BJ, Koeth R, Levison BS, DuGar B, Feldstein AE, Britt EB, Fu X, Chung Y-M, Wu Y, Schauer P, Smith JD, Allayee H, Tang WHW, DiDonato JA, Lusis AJ, Hazen SL, 2011. Gut flora metabolism of phosphatidylcholine promotes cardiovascular disease. Nature 472, 57–63. 10.1038/nature09922 [PubMed: 21475195]

Wikoff WR, Anfora AT, Liu J, Schultz PG, Lesley SA, Peters EC, Siuzdak G, 2009. Metabolomics analysis reveals large effects of gut microflora on mammalian blood metabolites. Proc. Natl. Acad. Sci 106, 3698–3703. 10.1073/pnas.0812874106 [PubMed: 19234110]

Wolfe RR, 1984. Tracers in metabolic research: radioisotope and stable isotope/mass spectrometry methods. Lab. Res. Methods Biol. Med 9, 1–287. [PubMed: 6427541]

Wong JMW, Jenkins DJA, 2007. Carbohydrate Digestibility and Metabolic Effects. J. Nutr 137, 2539S–2546S. 10.1093/jn/137.11.2539S [PubMed: 17951499]

Wühr M, Freeman RM, Presler M, Horb ME, Peshkin L, Gygi SP, Kirschner MW, 2014. Deep Proteomics of the Xenopus laevis Egg using an mRNA-Derived Reference Database. Curr. Biol 24, 1467–1475. 10.1016/j.cub.2014.05.044 [PubMed: 24954049]

Yasuda K, Oh K, Ren B, Tickle TL, Franzosa EA, Wachtman LM, Miller AD, Westmoreland SV, Mansfield KG, Vallender EJ, Miller GM, Rowlett JK, Gevers D, Huttenhower C, Morgan XC, 2015. Biogeography of the Intestinal Mucosal and Lumenal Microbiome in the Rhesus Macaque. Cell Host Microbe 17, 385–391. 10.1016/j.chom.2015.01.015 [PubMed: 25732063]

Yoshimoto S, Loo TM, Atarashi K, Kanda H, Sato S, Oyadomari S, Iwakura Y, Oshima K, Morita H, Hattori M, Honda K, Ishikawa Y, Hara E, Ohtani N, 2013. Obesity-induced gut microbial metabolite promotes liver cancer through senescence secretome. Nature 499, 97–101. 10.1038/nature12347 [PubMed: 23803760]

Zhang X, Ning Z, Mayne J, Deeke SA, Li J, Starr AE, Chen R, Singleton R, Butcher J, Mack DR, Stintzi A, Figeys D, 2016a. In Vitro Metabolic Labeling of Intestinal Microbiota for Quantitative Metaproteomics. Anal. Chem 88, 6120–6125. 10.1021/acs.analchem.6b01412 [PubMed: 27248155]

Zhang X, Ning Z, Mayne J, Moore JI, Li J, Butcher J, Deeke SA, Chen R, Chiang C-K, Wen M, Mack D, Stintzi A, Figeys D, 2016b. MetaPro-IQ: a universal metaproteomic approach to studying human and mouse gut microbiota. Microbiome 4, 31. 10.1186/s40168-016-0176-z [PubMed: 27343061]

Zhao S, Jang C, Liu J, Uehara K, Gilbert M, Izzo L, Zeng X, Trefely S, Fernandez S, Carrer A, Miller KD, Schug ZT, Snyder NW, Gade TP, Titchenell PM, Rabinowitz JD, Wellen KE, 2020. Dietary fructose feeds hepatic lipogenesis via microbiota-derived acetate. Nature 579, 586–591. 10.1038/s41586-020-2101-7 [PubMed: 32214246]

- Gut microbiome feedstocks mapped by isotope tracing into bacteria-specific peptides
- Major contributors are dietary fiber and protein, and host lactate, urea, and mucins
- Microbiome composition shifts towards bacteria fed their preferred nutrients
- Microbial metabolites' systemic levels reflect dietary precursors reaching microbiome

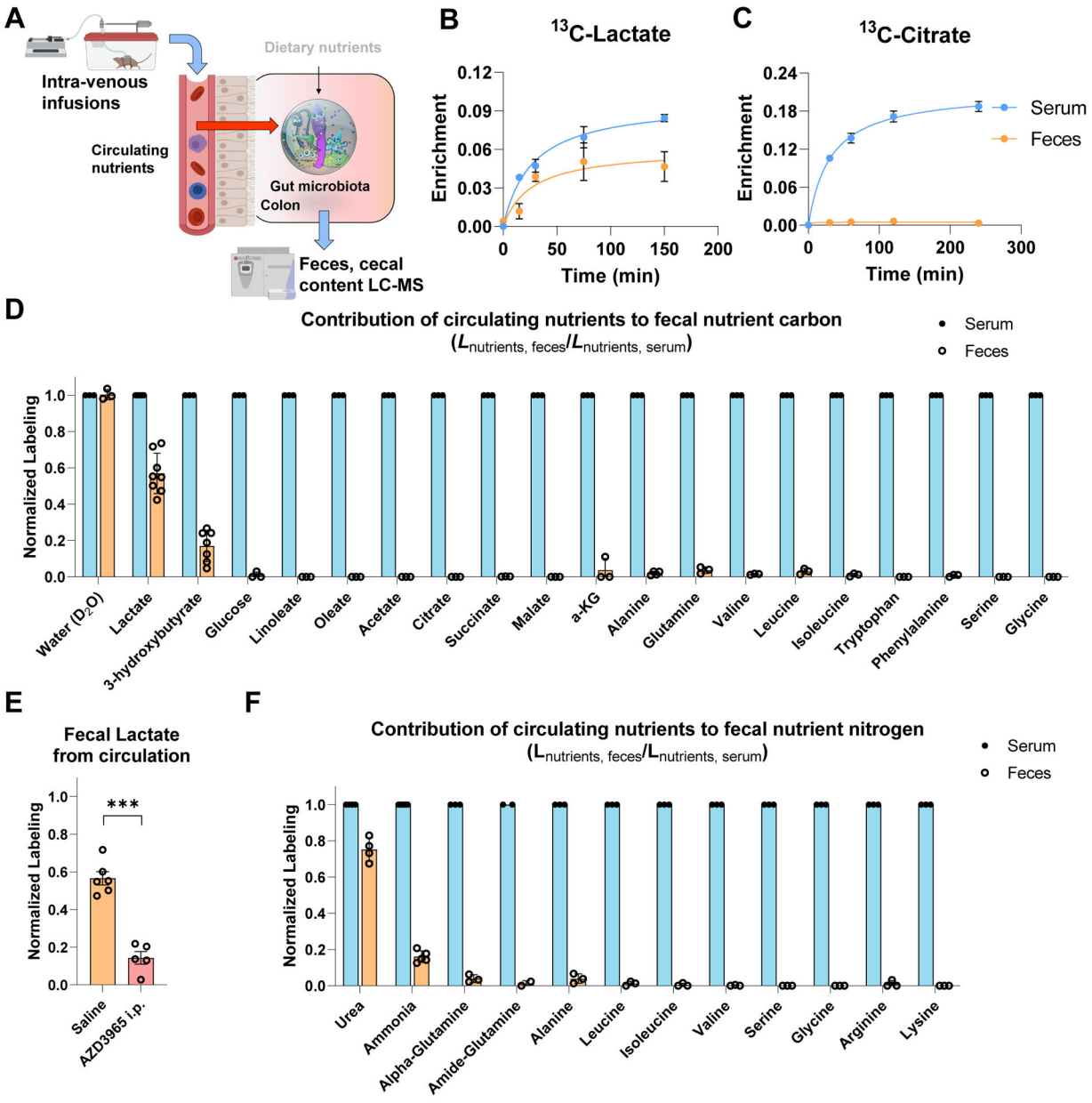

Figure 1. Circulating lactate and 3-hydroxybutyrate feed the gut microbiome. See also[Figure S2].

(A) Schematic of intravenous infusion of isotope-labeled nutrients to identify circulating metabolites that feed gut microbiome.

(B) Circulating lactate rapidly enters the feces. Mice were infused with ^{13}C-lactate and serum and fresh feces enrichment were compared. Mean±s.e., N = 3.

(C) Circulating citrate does not enter the feces. As in (B), for ^{13}C-citrate. Mean±s.e., N = 3.

(D) Passage of circulating ^{13}C-labeled nutrients into the feces. Mice were infused with labeled nutrients for 2.5 h, and labeling fraction in feces was normalized to labeling fraction in serum. Mean±s.e., N = 3 except for lactate (N = 8) and 3-hydroxybutyrate (N = 7).

(E) Pharmacological inhibition of MCT1 transporter decreases the passage of circulating lactate to feces. Mice were injected i.p. with saline or 100 mg/kg AZD3965, and fresh

feces lactate enrichment measured. Mean±s.e. N = 6 for saline and N = 5 for AZD3965. ***P<0.001 by two-sided Student's t-test.

(F) Passage of circulating ^{15}N-labeled nutrients into the feces. As in (D), for ^{15}N-lableing. Mean±s.e. N = 3 except for urea (N = 4) and ammonia (N = 5).

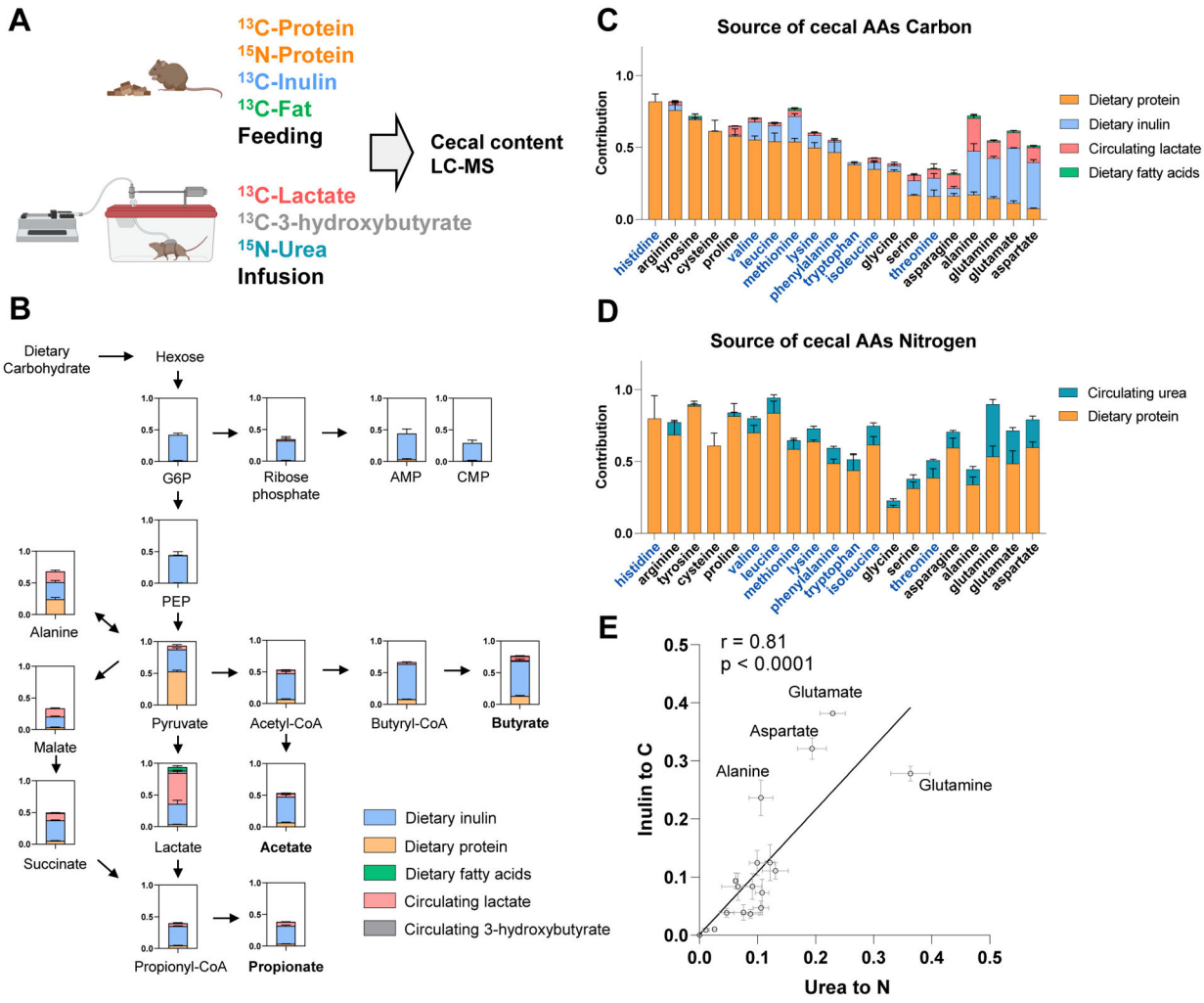

Figure 2. Quantitative analysis of dietary and circulating nutrient contributions to gut microbiome. See also Figure S3,S4.

(A) Experimental design. Mice were fed chow containing ^{13}C-protein, ^{13}C-inulin, ^{13}C-fatty acids, or ^{15}N-protein for 24 h. Alternatively, mice were intravenously infused with ^{13}C-lactate, ^{13}C-3-hydroxybutyrate or ^{15}N-urea for 24 h. The labeling of cecal content metabolites was analyzed by LC-MS.

(B) Contribution of dietary and circulating nutrients to carbohydrate fermentation pathways in gut microbiome. Mean ± s.e. N = 4.

(C) Contribution of dietary and circulating nutrients to cecal amino acid carbon. The names of essential amino acids (EAA) are written in blue and non-essential amino acids (NEAA) in black. Mean ± s.e. N = 4.

(D) Contribution of dietary and circulating nutrients to cecal amino acid nitrogen. As in (C), for nitrogen.

(E) Positive correlation, across amino acids in the cecal contents, of carbon contribution from dietary inulin and nitrogen contribution from circulating urea. Mean ± s.e. N = 4.

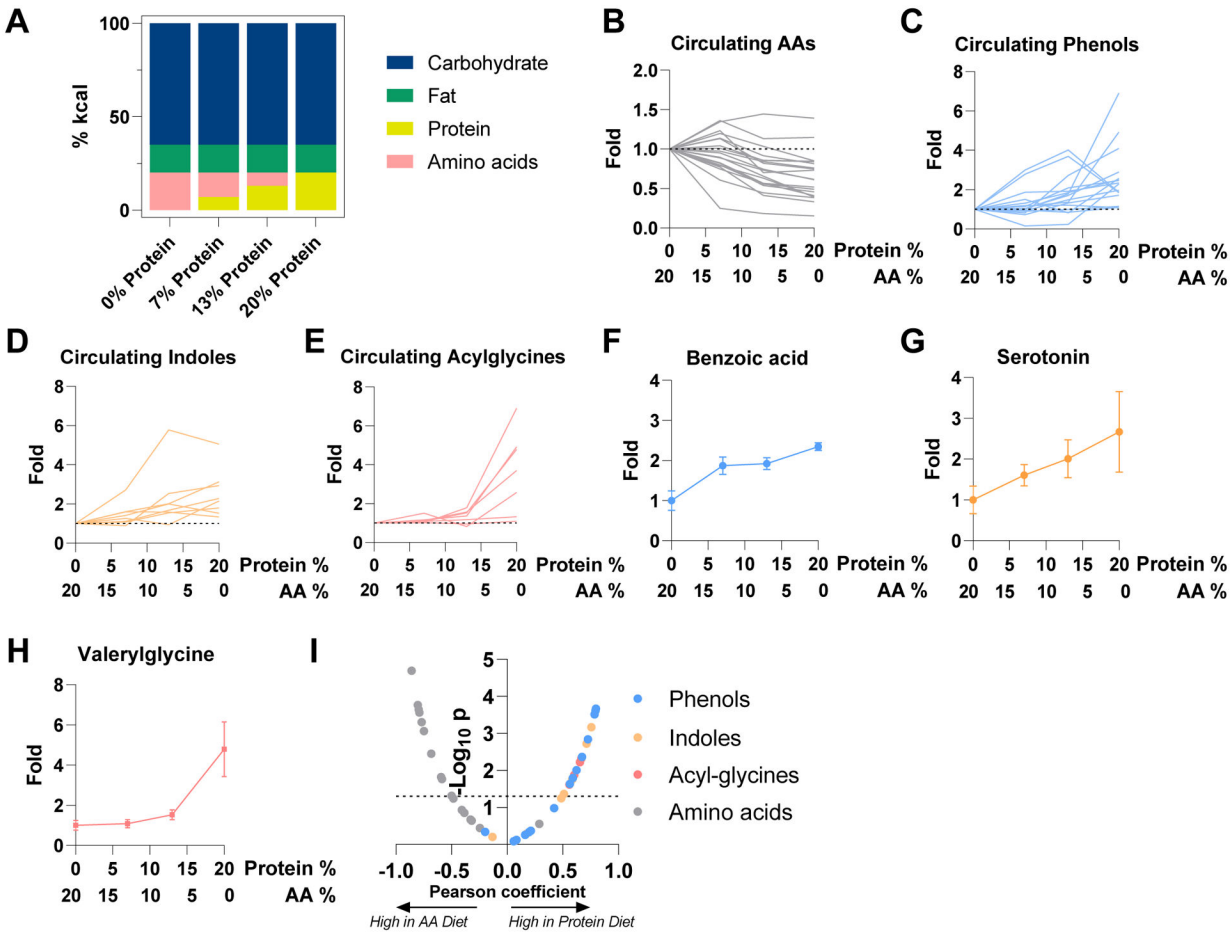

Figure 3. Circulating levels of microbiota metabolites depend on protein reaching the microbiome.

(A) Compositions of diets used in the figure. “Protein” is casein. “Amino acids” are composition-matched free amino acids.

(B) Concentration of circulating amino acids in systemic circulation after two weeks test diet relative to free amino acids diet. Serum was taken at *ad lib* fed state. Each metabolite is a line. Mean, N = 4 mice.

(C) As in (B), for phenols. Mean, N = 4 mice.

(D) As in (B), for indoles. Mean, N = 4 mice.

(E) As in (B), for acylglycines. Mean, N = 4 mice.

(F) As in (B) for benzoic acid. Mean ± s.e., N = 4 mice.

(G) As in (F), for serotonin. Mean ± s.e., N = 4 mice.

(H) As in (F), for valerylglycine. Mean ± s.e., N = 4 mice.

(I) Correlation between dietary protein (as opposed to free amino acid) fraction in diet and metabolite abundances (relative to amino acid diet). The volcano plot shows Pearson coefficient and P value of correlation between metabolite levels to casein abundance in diet.

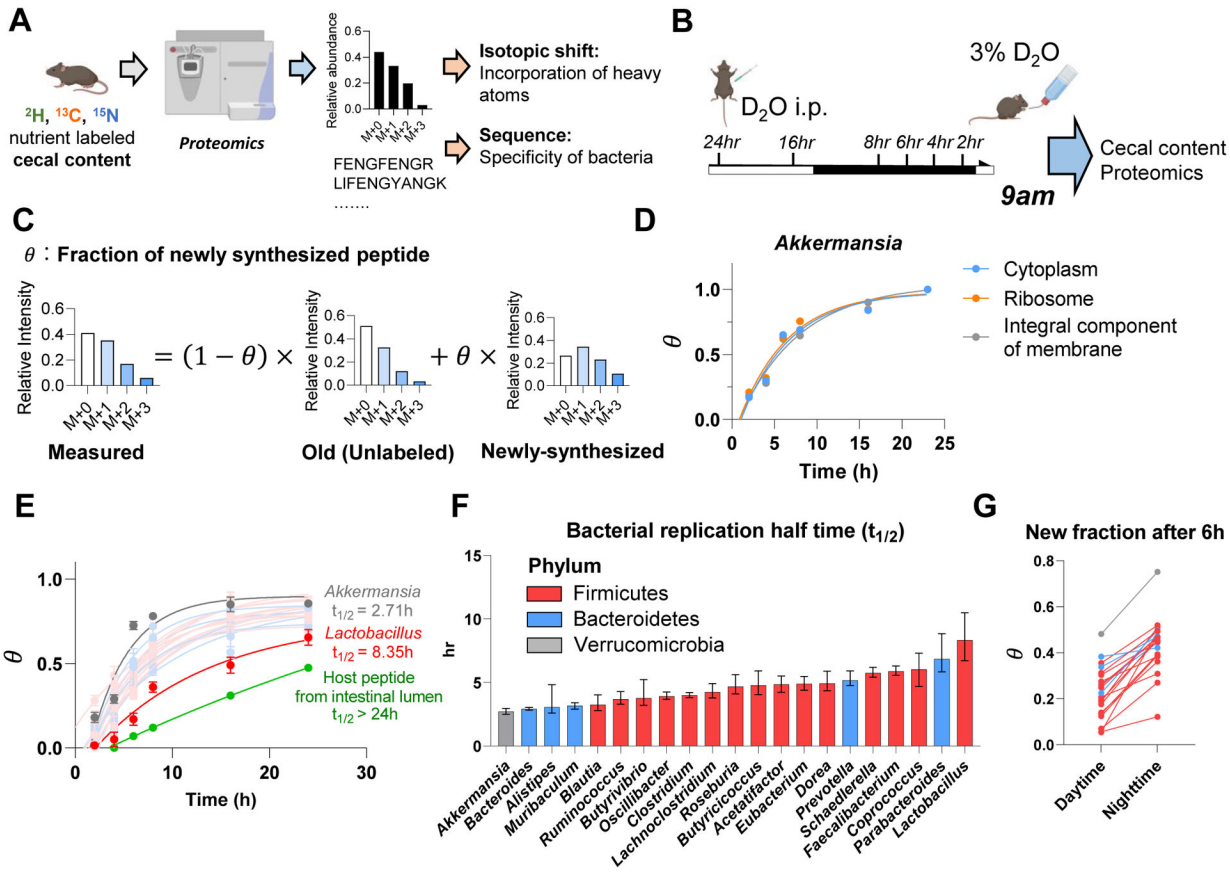

Figure 4. Growth rate of different gut bacterial genera quantified by isotope tracing. See also Figure S5.

(A) Experimental approach for isotope tracing into specific gut bacteria. Only peptides that are specific to a particular bacterial genus were examined.

(B) Growth rate quantification using D_2O. Mice received D_2O by i.p. injection followed by D_2O drinking water and cecal content labeling was measured over time by proteomics and metabolomics. Mice were fed *ad lib*; tissues were harvested at 9am.

(C) Calculation of newly synthesized peptide fraction (θ). The experimentally observed peptide mass isotope distribution was fit to a linear combination of unlabeled peptide ("old," heavy forms from natural isotope abundance) and newly synthesized peptide ("new," heavy forms from isotope labeling pattern of free cecal amino acids and from natural isotope abundance).

(D) Different cellular compartments from the same bacterial genus show similar labeling rate. Mean, N = 5 mice for each time point.

(E) Genus-specific growth rates were determined by a single exponential fitting, as a function of time, of θ (mean across both different peptides measured from that genus and replicate mice). Mean±s.e., N = 5 mice for each time point.

(F) Bacterial replication half time of different gut bacteria. Data are exponential fits ±s.e.

(G) The gut bacteria synthesize protein in sync with the physiological feeding patterns of the host. The figure shows the average newly synthesized peptide fraction (θ) for different gut bacterial genera after D_2O labeling during daytime vs nighttime. Each line connects the

daytime and nighttime measurements for one genus. Mean, N = 5 mice for daytime and for nighttime.

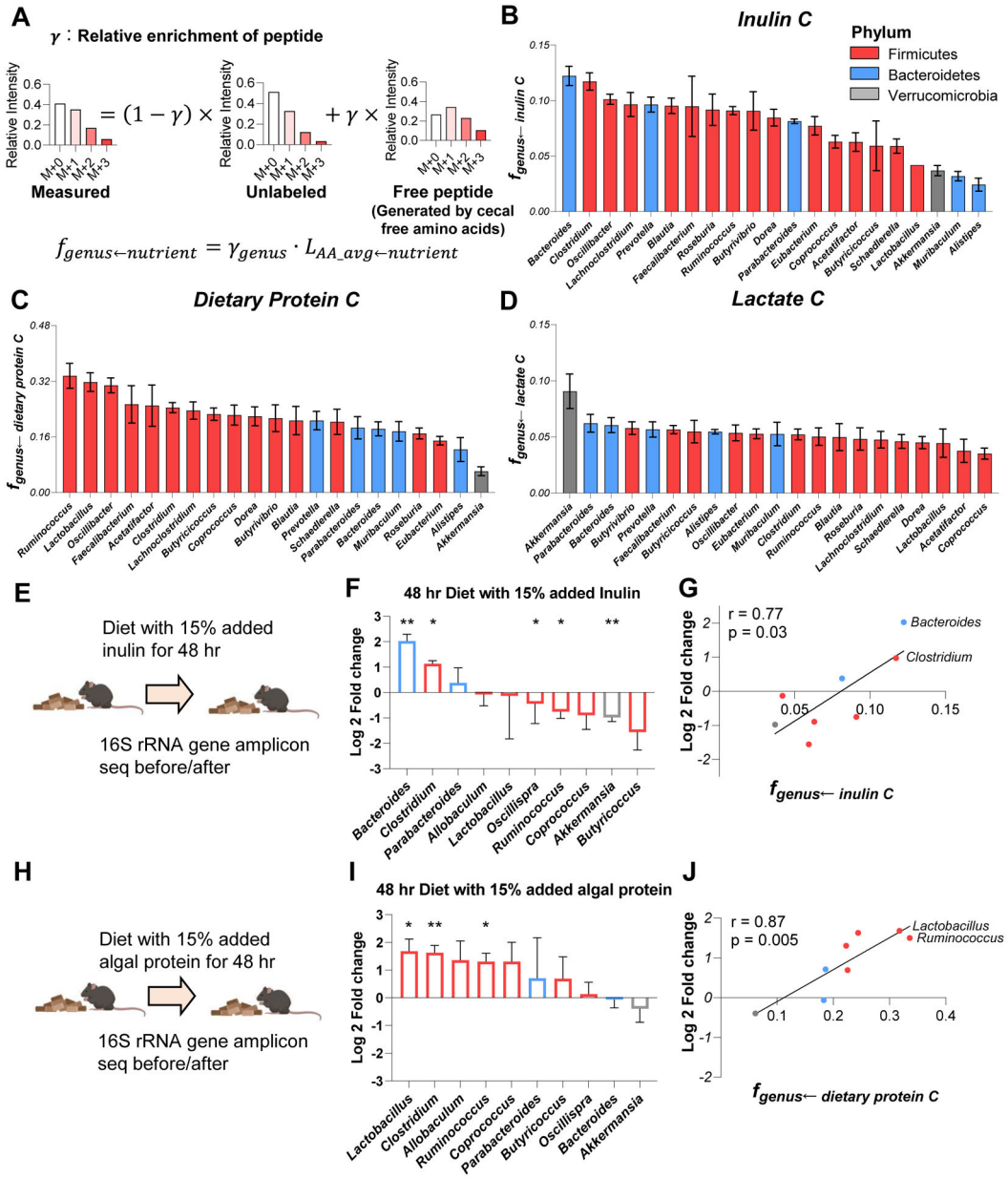

Figure 5. Preferred carbon sources differ across gut bacteria. See also[Figure S6].

(A) Calculation of peptide relative ^{13}C-enrichment (γ) and carbon contribution from the tracer to a bacterial genus ($f_{genus\leftarrow nutrient}$). First, the experimentally observed peptide mass isotope distribution was fit to a linear combination of unlabeled peptide (heavy forms from natural isotope abundance) and a peptide made from free cecal amino acids (heavy forms from isotope labeling pattern of free cecal amino acids and from natural isotope abundance), yielding. Then, $f_{genus\leftarrow nutrient}$ was determined by correcting for the fractional contribution of that tracer to the cecal free amino acid pools.

(B) Carbon contribution of dietary inulin across bacterial genera. Mean±s.e., N = 4 mice.

(C) Carbon contribution of dietary algal protein across bacterial genera. Mean±s.e., N = 6 mice.

(D) Carbon contribution of circulating lactate across bacterial genera. Mean±s.e., N = 7 mice.

(E) Experimental scheme of high-inulin diet feeding followed by 16S rRNA gene amplicon sequencing.

(F) Genus-level microbiota composition changes after high-inulin diet. The genera increased after high-inulin diet prefer inulin in (B). Mean±s.e., N=3 mice. *P<0.05 and **P<0.01 by two-sided Student's t-test.

(G) Correlation between genera abundance changes and carbon-source preference.

(H- J) As in (E - G), for algal protein-supplemented diet.

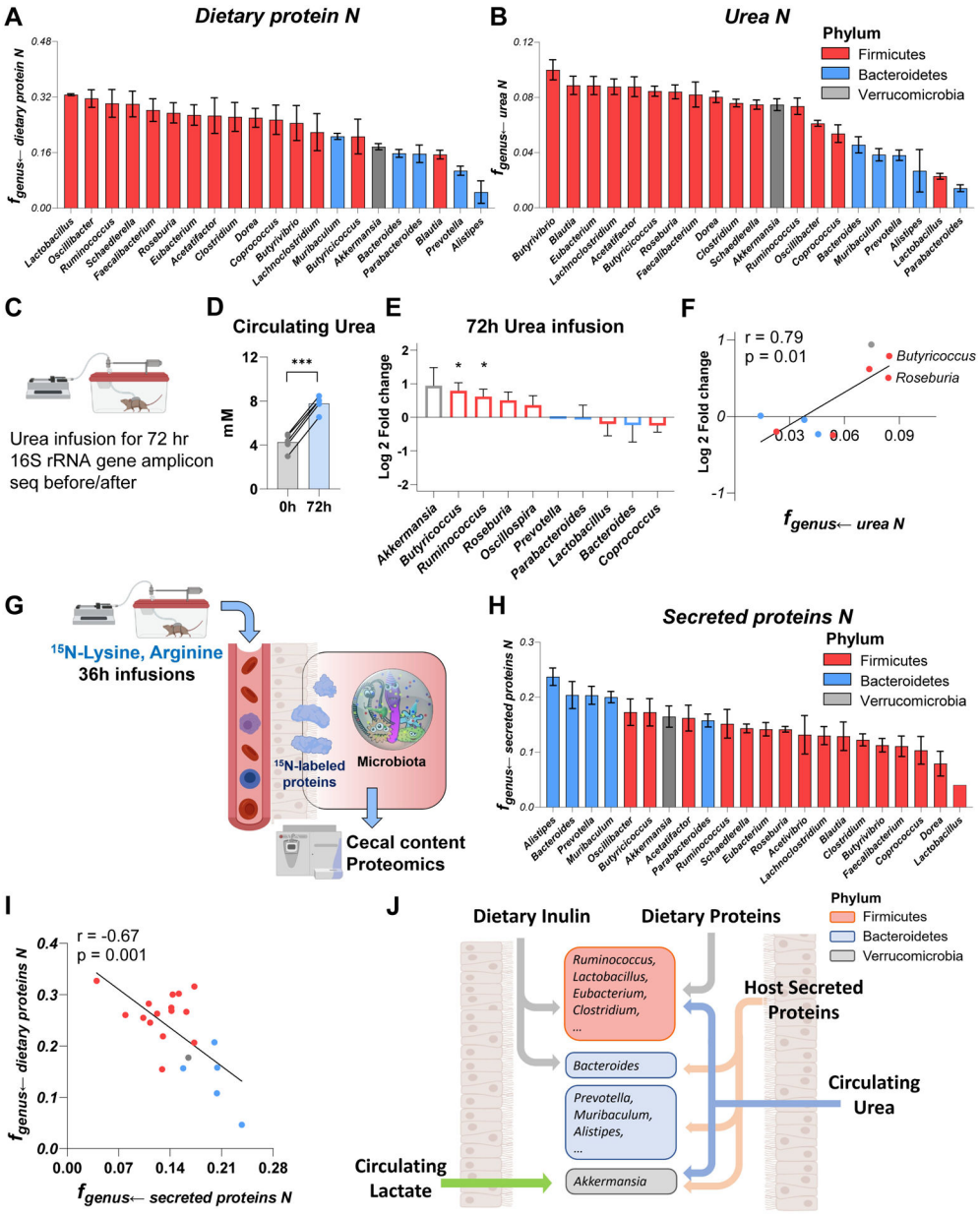

Figure 6. Firmicutes favor dietary protein while Bacteroidetes prefer secreted host protein. See also Figure S6,S7.

(A) Nitrogen contribution of dietary algal protein across bacterial genera. Mean±s.e., N = 6 mice.

(B) Nitrogen contribution of circulating urea across bacterial genera. Mean±s.e., N = 6 mice.

(C) Experimental scheme of 72 hr urea infusion followed by 16S rRNA gene amplicon sequencing.

(D) Urea infusions increased urea concentration in systemic circulation. N = 5 mice. ***P<0.001 by two-sided Student's t-test.

(E) Genus-level microbiota composition changes after urea infusion. The genera increased after urea infusion prefer urea in (B). Mean±s.e., N=5 mice. *P<0.05 by two-sided Student's t-test.

(F) Correlation between genera abundance changes and nitrogen-source preference.
(G) Experimental schematic of long-term ^{15}N-lysine and ^{15}N-arginine infusion to probe the contribution of secreted host proteins to different bacterial genera.
(H) Nitrogen contribution of secreted host proteins across bacterial genera. Mean±s.e., N = 5 mice.
(I) Negative correlation between $f_{genus \leftarrow dietary\ proteins\ N}$ and $f_{genus \leftarrow secreted\ proteins\ N}$.
(J) Summary of carbon and nitrogen inputs to different gut bacteria. Firmicutes prefer dietary carbon sources (fiber and protein) and nitrogen from host circulating urea. Bacteroidetes heavily use dietary fiber, while using on host secreted proteins for nitrogen. Verrucomicrobia prefers host secreted nutrients, both protein and circulating small molecules (lactate, urea).

Table 1.

Absolute concentrations and sources of microbiota-associated metabolites. See also[Table S1,Figure S1,S4].

Data are from ad lib fed state (ZT0); for ad lib fasted state (ZT12), see Supplementary Table S1. Absolute concentration is mean, N = 5 mice. Portal/systemic = fold-change in concentration between the portal vein and tail vein (median, N = 5 mice). Abx/Conv refers to fold-change in portal blood concentration between mice treated with antibiotics cocktail versus not (median, N = 5 mice/group). Source bar indicates the relative contribution to the indicated metabolite from dietary inulin, algal protein and circulating lactate (based on

isotope tracing). Percentages indicate quantitative relative contributions from those nutrients (median, N = 4). Numbers typically add up to less than 100%, as other sources (e.g., mucins) contribute.

Metabolite	Systemic Concentration (μM)	Portal/Systemic (Log 2)	Abx/Conv (Log 2)	Source	Dietary Fiber	Dietary Protein	Circulating lactate
Acetate	210.0	3.1	-1.9		41%	8%	7%
Phenol	23.0	0.1	-4.3		0%	41%	0%
Indoxyl sulfate	22.0	-0.2	<-5.0		0%	13%	0%
Serotonin	12.0	-0.5	-1.4		0%	12%	0%
Propionate	9.9	>5.0	<-5.0		28%	4%	6%
4-Methylvaleric acid	7.3	0.5	-0.1		6%	43%	2%
Indole-3-acetic acid	7.2	-0.3	-0.9		0%	23%	0%
Phenyl sulfate	6.6	-0.5	<-5.0		0%	42%	0%
Acetylglycine	5.4	0.2	-0.2		29%	22%	0%
4-Ethylphenol	5.2	0.2	-0.9		0%	23%	0%
Indole-3-propionate	4.6	0.0	<-5.0		0%	26%	0%
Hippuric acid	4.2	0.3	-4.4		0%	33%	0%
4-Cresol	4.2	0.6	-0.4		0%	18%	0%
Indole-3-acetylaldehyde	4.1	-0.3	-0.2		0%	13%	0%
Trimethylamine-N-oxide	3.8	0.3	-3.8	Others	0%	0%	0%
Butyrate	3.6	>5.0	<-5.0		54%	13%	7%
Isobutyrate	2.8	2.8	-4.1		5%	35%	1%
2-Methylbutyrate	2.8	1.4	-3.0		5%	48%	1%
Catechol	2.8	0.0	<-5.0	Others	0%	0%	0%
5-Aminovaleric acid	2.0	0.4	-0.3		0%	14%	0%
Indole-3-lactic acid	1.9	0.8	-0.7		0%	27%	0%
3-Hydroxycinnamic acid	1.6	-0.1	-0.6		0%	29%	0%
3-Phenylpropionate	1.5	2.4	-5.0		0%	22%	0%
Isovaleric acid	1.2	2.9	-3.7		1%	45%	1%
Benzoic acid	1.2	0.3	<-5.0		0%	32%	0%
Valerate	1.1	4.9	-3.8		6%	37%	5%
Cinnamoylglycine	1.1	0.7	-1.1		0%	39%	0%
Inosine	1.1	-3.3	0.4		12%	11%	0%
Phenylacetic acid	0.79	0.6	-2.8		0%	50%	0%
4-Hydroxyphenylpropionate	0.76	0.2	-2.0		0%	56%	0%
Propionylglycine	0.75	1.2	-0.1		21%	24%	0%
Phenylpropionylglycine	0.75	0.6	-0.3		2%	22%	0%
Heptanoic acid	0.74	0.6	-0.3		6%	11%	0%
Indole	0.53	0.2	-2.6		0%	49%	0%
Butyrylglycine	0.39	1.1	-1.4		37%	28%	0%
4-Hydroxylphenylacetate	0.37	0.7	-1.0		0%	32%	0%
N-Acetyl-Tryptophan	0.37	0.1	0.5		0%	13%	0%
Tauroursodeoxycholic acid	0.33	2.9	-2.2		0%	0%	0%
4-Hydroxybenzoic acid	0.25	0.7	-1.0		0%	9%	0%
Cinnamic acid	0.20	2.5	-2.6		0%	41%	0%
Taurodeoxycholic acid	0.11	4.8	-3.1		0%	0%	0%
2-Hydroxyhippuric acid	0.062	1.5	-0.7		0%	22%	0%
Imidazole propionate	0.051	0.7	-0.7		0%	37%	0%
Deoxycholic acid	0.048	3.1	<-5.0		0%	0%	0%
Indole-3-ethanol	0.032	1.6	-0.3		0%	38%	0%
Ursodeoxycholic acid	0.026	2.5	<-5.0		0%	0%	0%
4-Cresol sulfate	0.026	-0.2	-2.8		0%	26%	0%
Phenylacetylglycine	0.017	0.2	-0.3		0%	32%	0%
Equol	0.013	3.7	<-5.0	Others	0%	0%	0%
Hyodeoxycholic acid	0.009	3.0	-3.7		0%	0%	0%
Lithocholic acid	0.008	1.8	<-5.0		0%	0%	0%
Taruolithocholic acid	<0.001	>5.0	<-5.0		0%	0%	0%
Isoallolithocholic acid	<0.001	>5.0	<-5.0		0%	0%	0%
Glycoursodeoxycholic acid	<0.001	>5.0	-4.5		0%	0%	0%
Glycodeoxycholic acid	<0.001	>5.0	-1.3		0%	0%	0%

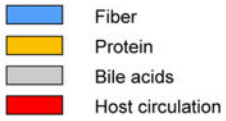

Key Resources Table

REAGENT or RESOURCE	SOURCE	IDENTIFIER
Chemicals, Peptides, and Recombinant Proteins		
DEUTERIUM OXIDE (D, 99.9%)	Cambridge Isotope Laboratories	Cat# DLM-4-PK
D-GLUCOSE (U-13C6, 99%)	Cambridge Isotope Laboratories	Cat# CLM-1396-PK
SODIUM L-LACTATE (13C3, 98%) 20% W/W in H2O	Cambridge Isotope Laboratories	Cat# CLM-1579-PK
L-GLUTAMINE (13C5, 99%)	Cambridge Isotope Laboratories	Cat# CLM-1822-H-PK
L-GLUTAMINE (ALPHA-15N, 98%)	Cambridge Isotope Laboratories	Cat# NLM-1016-PK
L-GLUTAMINE (AMIDE-15N, 98%+)	Cambridge Isotope Laboratories	Cat# NLM-557-PK
SODIUM D-3-HYDROXYBUTYRATE (13C4, 99%) 97% CHEMICAL PURITY	Cambridge Isotope Laboratories	Cat# CLM-3853-PK
LINOLEIC ACID, POTASSIUM SALT (U-13C18, 98%)	Cambridge Isotope Laboratories	Cat# CLM-8835-PK
OLEIC ACID, SODIUM SALT (U-13C18, 98%)	Cambridge Isotope Laboratories	Cat# CLM-8763-PK
SODIUM PALMITATE (U-13C16, 98%+)	Cambridge Isotope Laboratories	Cat# CLM-6059-PK
SODIUM ACETATE (1,2–13C2, 99%)	Cambridge Isotope Laboratories	Cat# CLM-440-PK
CITRIC ACID (13C6, 99%)	Cambridge Isotope Laboratories	Cat# CLM-9021-PK
SUCCINIC ACID (13C4, 99%)	Cambridge Isotope Laboratories	Cat# CLM-1571-PK
L-MALIC ACID (13C4, 99%)	Cambridge Isotope Laboratories	Cat# CLM-8065-PK
ALPHA-KETOGLUTARIC ACID, DISODIUM SALT (1,2,3,4–13C4, 99%)	Cambridge Isotope Laboratories	Cat# CLM-4442-PK
L-ALANINE (13C3, 99%)	Cambridge Isotope Laboratories	Cat# CLM-2184-H-PK
L-ALANINE (15N, 98%)	Cambridge Isotope Laboratories	Cat# NLM-454-PK
L-VALINE (13C5, 99%)	Cambridge Isotope Laboratories	Cat# CLM-2249-H-PK
L-VALINE (15N, 98%)	Cambridge Isotope Laboratories	Cat# NLM-316-PK
L-LEUCINE (13C6, 99%)	Cambridge Isotope Laboratories	Cat# CLM-2262-H-PK
L-LEUCINE (15N, 98%)	Cambridge Isotope Laboratories	Cat# NLM-142-PK
L-ISOLEUCINE (13C6, 99%)	Cambridge Isotope Laboratories	Cat# CLM-2248-H-PK
L-ISOLEUCINE (15N, 98%)	Cambridge Isotope Laboratories	Cat# NLM-292-PK

REAGENT or RESOURCE	SOURCE	IDENTIFIER
L-SERINE (13C3, 99%; 15N, 99%)	Cambridge Isotope Laboratories	Cat# CNLM-474-H-PK
GLYCINE (13C2, 97–99%)	Cambridge Isotope Laboratories	Cat# CLM-1017-PK
GLYCINE (13C2, 99%; 15N, 99%)	Cambridge Isotope Laboratories	Cat# CNLM-1673-H-PK
L-TYROSINE (13C9, 99%)	Cambridge Isotope Laboratories	Cat# CLM-2263-H-PK
UREA (15N2, 98%+)	Cambridge Isotope Laboratories	Cat# NLM-233-PK
AMMONIUM CHLORIDE (15N, 99%)	Cambridge Isotope Laboratories	Cat# NLM-467-PK
L-LYSINE:2HCL (ALPHA-15N, 98%)	Cambridge Isotope Laboratories	Cat# NLM-143-PK
L-ARGININE:HCL (ALPHA-15N, 98%+)	Cambridge Isotope Laboratories	Cat# NLM-1267-PK
ALGAL STARCH (U-13C, 98%+)	Cambridge Isotope Laboratories	Cat# CLM-1699-PK
INULIN (FROM CHICORY) (U-13C, 97%+) 97% CHEMICAL PURITY	Cambridge Isotope Laboratories	Cat# CLM-9181-PK
Algal crude protein extract-13C	Sigma-Aldrich	Cat# 642878
Algal crude protein extract-15N	Sigma-Aldrich	Cat# 586773
Algal crude protein extract-13C,15N	Sigma-Aldrich	Cat# 608254
Algal amino acid mixture-13C	Sigma-Aldrich	Cat# 426199
Algal fatty acid mixture-13C	Sigma-Aldrich	Cat# 487937
AZD 3965	AstraZeneca	Cat# AZD3965
Ampicillin	Sigma-Aldrich	Cat# A0166
Neomycin trisulfate salt hydrate	Sigma-Aldrich	Cat# N6386
Metronidazole	Sigma-Aldrich	Cat# M1547
Vancomycin hydrochloride from *Streptomyces orientalis*	Sigma-Aldrich	Cat# V1130
Trypsin	Promega	Cat# V5113
Lysyl endopeptidase R	Wako Chemicals USA	Cat# 12902541
Aspartame	Sigma-Aldrich	Cat# 47135
GAM Broth Modified	HyServe	Cat# 5433
LB Broth (Miller, Luria Broth)	Sigma	Cat# L3522
MRS Broth	Sigma	Cat# 69966
TSB (Tryptic Soy Broth)	Bacto	Cat# 211825
Experimental Models: Organisms/Strains		
Mouse: C57BL/6	Charles River Laboratories	Cat #027
Strain: *Bacteroides dorei* (CL02T00C15)	BEI	#HM-717
Strain: *Clostridium sporogenes* (ATCC 15579)	ATCC	15579
Strain: *Escherichia coli* (ATCC 25922)	ATCC	25922
Strain: *Lactobacillus reuteri* (CF-48–34A)	BEI	#HM-102
Strain: *Staphylococcus aureus subsp. Aureus Rosenbach*	ATCC	29213

REAGENT or RESOURCE	SOURCE	IDENTIFIER
Software and Algorithms		
El-MAVEN software	Elucidata	https://resources.elucidata.io/elmaven
AccuCor	GitHub	https://github.com/XiaoyangSu/AccuCor
PepMID	GitHub	https://github.com/xxing9703/pepMID_simul
MATLAB R2021b	MathWorks	N/A
Others		
PicoLab Rodent Diet 20	LabDiet	Cat# 5053
20% Diet premix	Research Diets	Cat# D11112201Npx2i
20% Amino acids diet	Research Diets	Cat# A11112201Bi